Abstract

When inspecting the currently known pulsar population one finds a velocity distribution which is in constrast to the galactic rotation curve. This has lead researchers to believe that the pulsars receive linear momentum (a kick) at the SN event which produces these. In this work we try and see what can be learned about these kicks by studying the existing double neutron star binary population. We investigate the possible progenitors to these and study their implications for the possible kicks. Furthermore we conduct a population synthesis and extrapolate from the statistics given by the current double neutron star population what is implied statistically regarding the angular kick distribution. We find that the population in fact implies a non-isotropic distribution with preference towards the orbital plane and we argue that the currently published kick probability distribution functions are too biased towards higher kick velocities.

Acknowledgements

I want to thank the Astronomy department for creating an excellent environment for a young student to learn and thrive in. Discussions I have had with various people showing concern and interest have been invaluable. I thank Prof. Melvyn Davies for lessons he probably never knew he taught me, and Adriaan Ludl for some contributions concerning the possibilities of Latex.

Of course, I thank Dr. Ross Church who has given me excellent supervision. In particular I am grateful for the discussions we had, but also the patience he showed when I wanted to do things my own way...

Contents

1 Introduction and overview

The first Double Neutron Star (DNS) binary was discovered by Hulse & Taylor (1975), a feat for which they were awarded the Nobel Prize later in 1993. The DNS binaries carry great scientific interest; not only are they very scarce, which in itself makes them interesting, but they relate to so many other relevant, highly topical and important astrophysical phenomena. As will be mentioned below, the DNS binaries are excellent laboratories for observations concerning General Relativity, with the gravitational wave physics. They are also important as they can provide constraints on the progenitors; both the formation channels as well as the supernova (SN) in which they are formed. The very likely progenitors of Short Gamma Ray Bursts (SGRB) might be DNS binaries.

In this work we set out to answer the question

- What can be learned about the kicks from the observed DNS binary sample? In particular, what can we learn about the kick angles?

In the first four chapters, the discussion concerns what is currently understood about DNS binaries. Section 2 regards how they are formed from *zams* binaries, Section 3 concerns the SN event itself, more specifically the kick, and Section 4 deals with the post-formation behavior.

The following chapters deals with the actual work done; Chapter 5 deals with deriving the necessary mathematics, which will be used in the simulations. Sections 6 and 7 deal with the simulations and description thereof, whereas the remaining section concludes the work and gives suggestions of how to further proceed with this work.

The remainder of this section is devoted to introducing what is actually known about the DNS binaries and NS kicks by direct observation.

1.1 Kick evidence

Dispersed throughout the galactic plane are pulsars with relatively high velocities, (see e.g. Lorimer (2008)). The galactic rotation, which has a velocity curve of $v_{rot} \approx 200\, km/s$[1] given in e.g. Sofue et al. (2009), does not correspond to these pulsar velocities which from e.g. Hansen & Phinney (1997) or Hobbs et al. (2005) have a mean of about 450 km/s. This suggests that they must receive some sort of "kick" at birth.

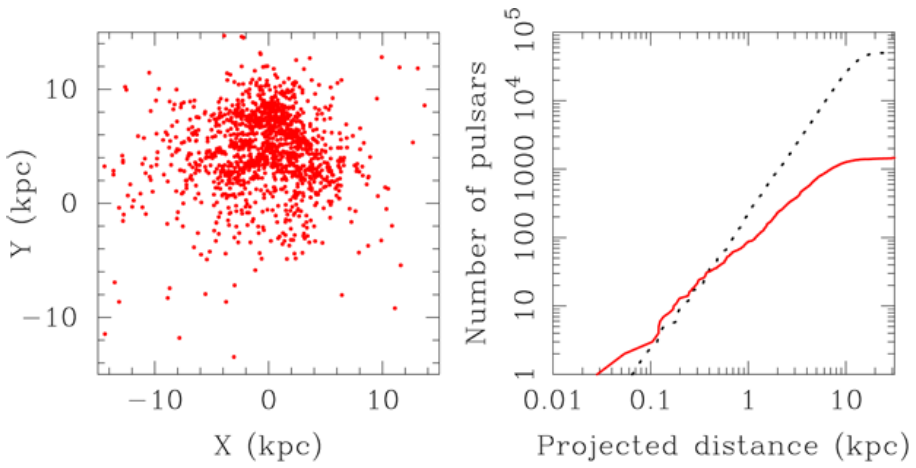

Figure 1: The pulsar demography as presented in Lorimer (2008).

[1]The Newtonian theory predicts a decline in velocity as the radius increases. What is measured is a "constant" velocity in radius (This is one of the main implications of exotic matter). The velocity is, of course, not perfectly constant, but varies a bit in the orbital plane with radius. The major deviation from the given rotational velocity occurs at higher radii than about 10 kpc. From Figure 1 taken from Lorimer (2008) one sees that the pulsar population is essentially concentrated within 10 kpc, where the rotational curve deviates less.

Note in Figure 1 the observational bias for pulsars towards the sun, placed roughly at $(0, 8.5)\,kpc$. As neutron stars are relatively faint objects they are relatively hard to detect at greater distances, which in turn gives rise to this selection effect. In reality, they probably follow a radially symmetric distribution.

1.2 Kick distribution

Studying the currently known pulsar population, various groups have found velocity distribution functions of the Maxwellian[1] type, both unimodal (Hansen & Phinney 1997), (Hobbs et al. 2005), as well as a bimodal distributions (Arzoumanian et al. 2002). The average velocities with respect to the local standard of rest are about $450\,km/s$ in the distributions.

The Arzoumanian et al. (2002) PDF was found by population synthesis followed by comparison with the known pulsar sample. The PDF has the following appearance:

$$P(v) = 4\pi v^2 \left[\frac{w_1}{(2\pi\sigma_{v_1}^2)^{3/2}} e^{-v^2/2\sigma_{v_1}^2} + \frac{(1-w_1)}{(2\pi\sigma_{v_2}^2)^{3/2}} e^{-v^2/2\sigma_{v_2}^2} \right]$$

where they found the best fit with $w_1 = 0.4$, $\sigma_{v_1} = 90\,km/s$ and $\sigma_{v_2} = 500\,km/s$.

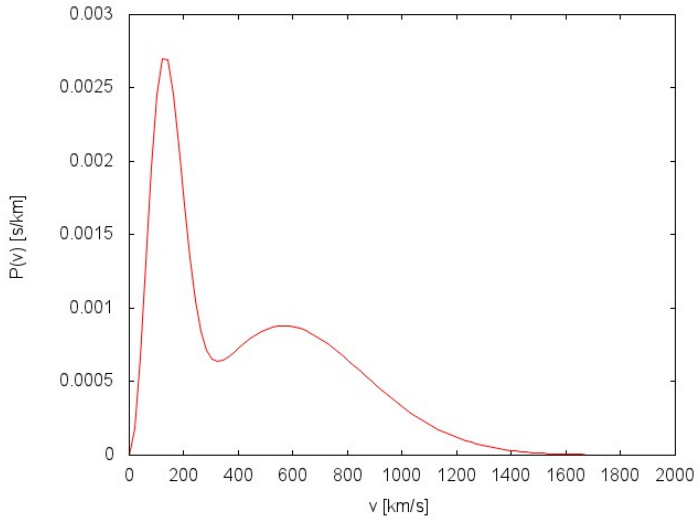

Figure 2: Plot of the PDF given by Arzoumanian et al. (2002).

There is, however, a slight ambiguity concerning the kick PDF; a later study by Hobbs et al. (2005) was conducted and resulted in a non-bimodal PDF. The bimodal PDF is attractive as it would be consistent with two different formation mechanisms for NS, which seems to be the case; e.g. Kiziltan et al. (2010) has measured bimodality between $M_{NS} \sim 1.35\,M_\odot$ and $M_{NS} \sim 1.50\,M_\odot$. This would hint of two different formation scenarios for DNS. It is currently believed that these two remnant masses are dependent on whether the system has been in a binary or not, (that is they have had the binary interactions of Roche-lobe overflow and then had their binary system broken by the kick). This conclusion has been reached as there are no single low-velocity NS.

1.3 The currently known DNS binaries

Throughout the below calculations and simulations, most of the data will be taken from Zhang et al. (2011) and Kiziltan et al. (2010), with references therein. Inspiral time will be taken from Lorimer (2008). The diversity of authors stems mainly from the fact that as observational techniques increase in accuracy, the data tend to change, and only in the latest years have many of the masses been measured with valuable accuracy.

[1]The PDFs of the type $P(v) \propto v^2 e^{-kv^2}$ are also denoted *Weibull-distributions*, but within physics literature the convention is to refer to these as Maxwellian.

Table 1 below presents the currently available data. Note that the binary $B1820-11$ is not a confirmed DNS binary and thus is not stated. For comparison with the merger time, the *Hubble Time* has $\tau_{Hubble} \approx 13.7\,Gyr$.

Table 1: Table of properties of the currently known DNS. The quantity P_{orb} denotes the binary orbital period. P_s denotes the pulsar spin frequency. Characteristic age is denoted by τ_c and merger time by $\tau_{inspiral}$. The pulsar mass is denoted M_{NS} with its binary companion mass being M_{comp}.

Designation	$P_{orb}\,[d]$	$P_s\,[ms]$	e	$\tau_c\,[Myr]$	$\tau_{inspiral}\,[Gyr]$	$M_{NS}\,[M_\odot]$	$M_{comp.}\,[M_\odot]$
J0737-3039 A	0.102	22.7	0.088	150	0.085	1.338 ± 0.01	1.249 ± 0.01
J0737-3039 B	0.102	2770	0.088	50	0.085	1.249 ± 0.01	1.338 ± 0.01
J1518+4904	8.63	40.9	0.25	20×10^3	>10	$1.56^{+.20}_{-1.25}$	$1.05^{+1.21}_{-0.14}$
J1811-1736	18.8	104.7	0.828	10^3	>10	$1.5^{+0.1}_{-0.25}$	$1.06^{+0.46}_{-0.15}$
J1829+2456	1.176	41.0	0.139	12.6×10^3	>10	$1.15^{+0.1}_{-0.25}$	$1.35^{+0.46}_{-0.15}$
B1534+12	0.421	37.9	0.274	400	2.7	1.33 ± 0.0020	1.35 ± 0.0020
B1913+16	0.323	59.0	0.617	100	0.3	1.44 ± 0.0006	1.39 ± 0.0006
B2127+11C	0.335	30.5	0.681	100	0.2	1.35 ± 0.080	1.36 ± 0.080
J1756-2251	0.320	28.5	0.181	400	1.7	$1.4^{+0.04}_{-0.06}$	$1.18^{+0.06}_{-0.04}$
J1906+0746	0.166	144	0.085	0.13	0.3	1.25	1.27

2 Formation channels

Since the discovery of the *Hulse-Taylor pulsar* in 1974 there have been various proposed formation channels for double neutron star binaries. Binary evolution is of course more a complicated task to study, as it depends on so much more than just the masses, as in the single component case. The most commonly adopted formation channel is the "Standard formation channel" by Bhattacharya & van den Heuvel (1991). This scenario, which will be explained below more in detail, will be adopted throughout this work. An alternate scenario proposed by Brown (1995), which is equally possible given somewhat special mass ratio conditions, will also be discussed.

2.1 The "standard channel"

The standard channel, depicted in Figure 3, assumes initially two close main sequence stars with masses in the range of $8\,M_\odot - 25\,M_\odot$. This is the mass range for which stars are believed to form NS as remnants (this is not as trivial in the binary case, as will be discussed below). The masses would correspond to a spectral classification of *Be*-type[1].

If the masses are different, the more massive companion will enter the red giant stage first. This would almost certainly give rise to mass transfer. Assuming the masses are different enough, the "heavy" star goes SN before the companion enters red giant phase. It receives a kick due to the SN. The effect on the companion by the ejecta is assumed not to be of significance, following the arguments in Fryxell & Arnett (1981). If the binary remains bound, it will now consist of a main sequence star and a neutron star (NS). Between the time of the first SN and the second red giant phase the main sequence star will lose mass through stellar wind, which in turn will be accreted onto the NS by *Bondi-Hoyle accretion*. This will result in the system becoming a High-Mass X-ray Binary, or HMXB for short.

The main sequence star then enters red giant phase where its hydrogen envelope expands. The NS will be engulfed by this and the system will share a common envelope (CE). Because of friction of the NS orbiting in the hydrogen gas, the envelope will receive some of its angular momentum and dissipate as the NS spirals in[2]. During this phase, the core and the NS might well merge depending on the initial separation and envelope mass. It is believed that to prevent merger the initial separation has to be at least $100\,R_\odot$. The situation can be explained somewhat more mathematically as follows. In the (CE) phase the envelope has potential and thermal energy. When the stars discard angular momentum and energy into the envelope, causing it to dissipate, they give it some of their Newtonian energy. In order to study what happens, one can equate the energy before and after CE-dissipation. Denote the separation before and after with a_f and a_i respectively. The energy before is given by

$$E_i = -G\frac{m_{MS}m_{NS}}{2a_i} + E_{env}$$

and after given simply by

$$E_f = -G\frac{m_{He}m_{NS}}{2a_f}$$

Denote the difference in orbital energy by ΔE_{orb} The problem here of course is to evaluate the final separation a_f as a function of initial separation a_i and the other parameters. The usual ansatz[3] is to try and formulate the envelope energy as a fraction of the pre-CE phase orbital energy, that is

$$E_{env} = -G\frac{m_{He}m_{env}}{\lambda a_i f(q)}$$

where the constant λ is a "free parameter" which is supposed to be determined by simulation and $f(q)$ is the well-known formula by Eggleton (1983) given by

$$f(q) = \frac{R_{L,1}}{a} = \frac{0.49q^{2/3}}{0.6q^{2/3} + \ln(1+q^{1/3})}, \qquad q = \frac{m_1}{m_2}$$

[1] Be-type are B-stars with strong H emission lines

[2] This can be visualized in two ways; either the NS "peels" of the envelope slowly, that is if the time-scale of the expansion of the CE is noncomparable to that of the mass expulsion, or the NS really becomes "engulfed" by the CE and lives as a tighter binary inside. Which of these scenarios is the actual case is still an open question.

[3] This is the famous "Webbink-formalism" (or "α_{CE}-formalism") after its introducer Webbink (1984). Note that the conventions are somewhat different here; e.g. instead of α_{CE} (the reason for the alternate name) there is η_{eff}.

and then equate this to the ΔE_{orb} modulo an efficiency parameter η_{eff} ranging between zero and one. That is $E_{env} = \eta_{eff}\Delta E_{orb}$.The efficiency parameter determines the capacity of the orbit to eject the envelope instead of heating it up. The energy can be evaluated just when the donor fills its Roche-lobe, that is $R_{MS} \approx R_L$. In Dewi & Tauris (2000) they find for various masses different values for λ.

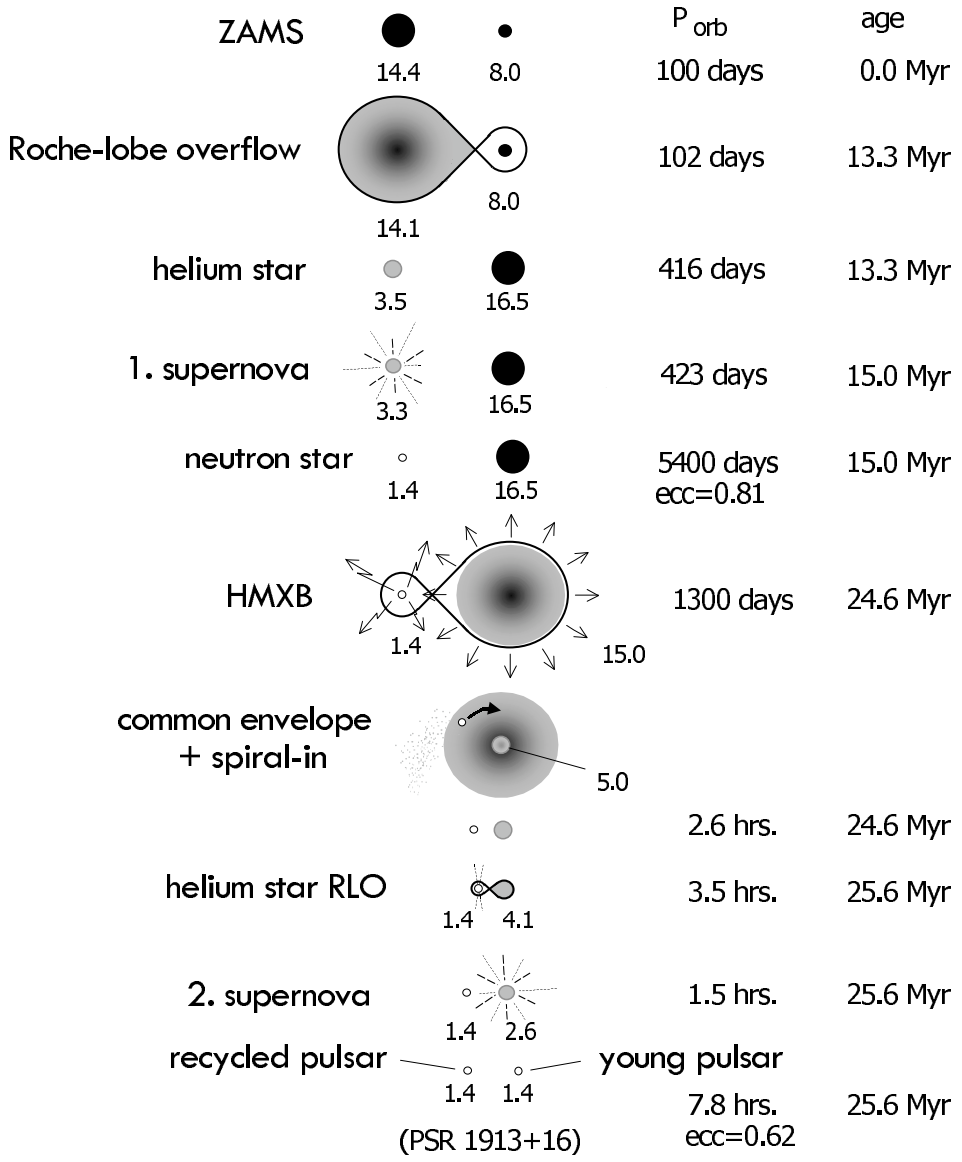

Figure 3: Depiction of the "standard channel". In this case it is illustrated by the probable formation scenario for $B1913$, the "Hulse-Taylor" pulsar. Courtesy of Tauris & van den Heuvel (2003)

This was done by equating the above ansatz for E_{env} to its classical energy

$$E_{bind} = \int_{M_{core}}^{M_{donor}} (-G\frac{M(r)}{r} + U)dm$$

That is to say, the envelopes binding energy as well as its thermodynamical energy. They reach typical values between 0.2 and 0.8 for λ, but also extreme cases with e.g. $\lambda > 5$. The quote of pre- and post-CE evolution separation can now be expressed as

$$\frac{a_f}{a_i} = \frac{m_{He}m_{NS}}{m_{MS}} \frac{1}{m_{NS} + 2m_{env}/(\eta_{eff}\lambda f(q))}$$

for typical values of the parameters, the ratio becomes of order ~ 100.

The scenario right up to the second supernova can safely be assumed to be circularized due to tidal interaction between the NS and the He-core. The timescale for this circularization can be estimated following Zahn (1989) to be

$$\frac{1}{t_{circ}} = 21\frac{\lambda_{circ}}{t_f}q(1+q)(\frac{R_{He}}{a})^8$$

where q the mass ratio, R_{He} the He-core radius, a the separation, $t_f = (m_1 R_{He}^2/L_{He})^{1/3}$ and λ_{circ} can be estimated with Zahns own recipe as $\lambda_{circ} \approx 0.019\alpha^{4/3}(1+\eta^2/320)^{-1/2}$, with $\eta = 2t_f/P_{orb}$. In Wang et al. (2006) they plugged in typical values and got t_{circ} to be of the order of a few hundreds of years. This is much shorter than to the time between the first and second SN, and thus assuming complete circularization before the second SN is correct.

The second SN will take place, and assuming that the second kick does not disrupt the binary it has now become a double neutron star binary. Just as in the case of the first SN, the ejecta will probably not be of significance as goes for the companion and will not be taken into account when constructing the mathematics in the below sections.

At the time this channel was proposed, it was thought that the NS would undergo *hypercritical accretion* during the CE-phase and as a result perhaps collapse into a BH. As now is known from the existing DNS binaries, the NS seldom exceed[1] masses of 1.5 $M_\odot$ and thus this cannot have happened. There has been proposed explanations for this. One of them being rotation as an inhibitor (Chevalier 1996); another that the accretion disc of the NS will give strong outflows (Armitage & Livio 2000).

2.2 The "double core channel"

An alternative formation channel, depicted in Figure 4, has been proposed by Brown (1995). Assuming that the zero age main sequence (ZAMS) stars have very similar masses they will enter the giant branch within very short time of each other. This is clearly not possible for the "standard channel" where the later companion has to SN before CE of the former companion. The allowed mass difference is in itself depending on the masses. In Dewi et al. (2006) they state that from single star models the allowed difference for stars of 8 $M_\odot$ is 3 %, and in case of 25 $M_\odot$ the allowed difference is 7 %. The stars will enter red giant phase within little time of each other, and thus form a double helium core binary within the CE. They will eject the hydrogen envelope through friction. This is also here calculated with the usual ansatz $E_{env} = \eta_{eff}\Delta E_{orb}$, where $\eta_{eff} \in (0,1)$ is the efficiency parameter. The orbital energy is as usual

$$E_{orb} = -G\frac{m_{core,1}m_{core,2}}{2a_f} + G\frac{m_{MS,1}m_{MS,2}}{2a_f}$$

The binding envelope energy is not the same as above, but restated as

$$E_{env} = -G\frac{m_{MS,1}m_{envelope,1}}{\lambda R_1} - G\frac{m_{MS,2}m_{envelope,2}}{\lambda R_2}$$

and as upon mass transfer the stellar radii can be approximated by their Roche-lobe radius R_L one can again use Eggletons formula with $R_L \approx af(q)$.

[1] See e.g. Lattimer & Prakash (2010) for recent reports on discoveries of massive NS with $m_{NS} = 2\,M_\odot$ or similar.

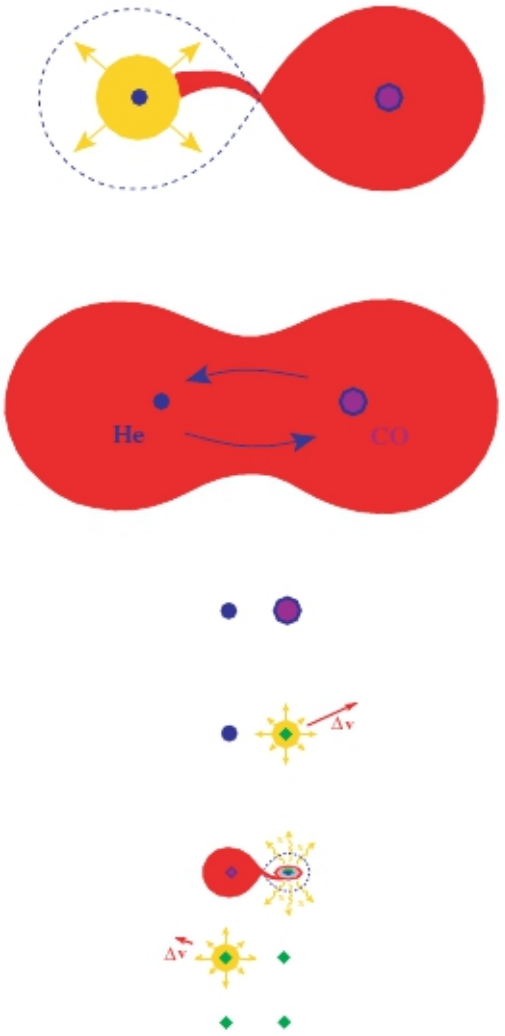

Figure 4: Depiction of the alternate formation channel. Courtesy of Dewi et al. (2006)

When the system has expelled the hydrogen CE there will remain a NS-He binary, just as in the standard channel. The He-core will undergo SN and there will remain two NS in a DNS binary.

2.3 Comparison

As the "double core" scenario is dependent on the sharp constraint on masses, it is the more unlikely scenario. The main difference between the two[1] channels is that in the "standard channel" the binary undergoes HMXB phase, whereas this does not occur in the "double core channel". In our below work we assume the former channel to have occurred.

[1] See e.g. Belczynski et al. (2002) for a rigorous comparison.

3 The kicks

Having an idea of how DNS binaries are formed we now move on to the kicks themselves. We start by discussing the currently popular mechanisms themselves and the proceed to discuss some related topics.

3.1 Mechanisms

Once established that formation seems to involve the remnant pulsar to receive a kick, various mechanisms have been proposed. The matter is to date not well understood and there has not yet been reached consensus.

As the neutron star is rather a heavy object and has a high velocity, there must be something compensating for its linear momentum. Today there are mainly two major mechanisms that explain this, while some other ones are considered exotic or unlikely. The major two are the *hydrodynamically driven* and *magneto-neutrino driven* mechanisms.

The *hydrodynamical mechanisms* is driven by asymmetries in the explosion. The shell has convective instabilities prior the the explosion resulting in an asymmetric bounce, so that the ejecta is asymmetric. Wongwathanarat et al. (2010) did 3D-simulations of this model and found that the produced kicks might well receive velocities $\sim 1000\,km/s$. They did not however, find that the SN altered spin angular momentum, or any preferred direction of the kick.

The *neutrino-driven* mechanism preserved linear momentum by asymmetric neutrino emission. Strong B-fields couple to the neutrinos and induce the asymmetric emission. Simulating the SN event and considering this mechanism, Fryer & Kusenko (2006) found that this mechanism could explain the observed velocities. Furthermore, they found that in contrast to the hydrodynamical mechanism, the ejecta and the pulsar velocities would in this scenario be *parallel*, instead of anti-parallel. Also it seems that the strength of the B-field has to be larger than the observed ones at $B \sim 10^7 - 10^{12}\,G$, at the magnitude of $B \sim 10^{15}\,G$.

3.2 Spin period- eccentricity relation

When studying the current DNS binaries in a $\log(P_s) - e$ -diagram one observes a linear relation between the variables. Using a very low kick-range [1] Dewi et al. (2005) found that this relation could be reproduced. This is taken as an implication of a low v_{kick} in the formation of DNS binaries. [2] It should be noted that there is still an uncertainty of this as there are very few known DNS binaries and thus more would be very useful.

3.3 Spin alignment

An important factor when constraining the kick angle is the spin-orbit misalignment, that is the angle between the orbital angular momentum vector L and the pulsar spin angular momentum vector S_{NS}. As intermediate-stage system undergoes Roche-lobe overflow, the spin vectors are aligned with the orbital angular momentum vectors. Although SN event might well change the spin of the younger pulsar, the older one remains undisturbed and can thus be used to provide constraints on the kick direction.

For some systems these angle have been measured, in particular in the tight binary system $J0737$. In Farr et al. (2011) these angles are given with no more than 14° for the older pulsar and 130° for the younger one, clearly showing that the SN must have altered the spin of the younger pulsar.

3.4 Various observed bimodalities

There are currently various bimodalities observed concerning the pulsar population, hinting of different formation channels. As stated above, there is bimodality in pulsar velocities, but there is also bimodalities in masses and spin alignments. In a study done by Kiziltan et al. (2010), they found that the masses of

[1] Maxwellian distribution with dispersion of $\sigma = 20\,km/s$

[2] Later in Willems et al. (2008) it was found that this relation could be maintained even with very polarly inclined kicks, albeit still not alleviating the need for a low kick-distribution.

the remnant NSs where bimodally distributed around $1.35\,M_\odot$ and $1.5\,M_\odot$. Furthermore, it has also been observed that NSs have bimodally distributed spin alignments (Johnston et al. 2005), being either very polarly inclined or planarly so. It has been argued that these bimodalities could be consistently explained if there were essentially two formation mechanisms for NSs; one being that the lower mass and low kick NS remnants originate from an electron capture SN having evolved in an interacting binary, whereas the other is a single star evolution (or non-interacting binary) of the progenitor with a somewhat higher zams mass ($\sim 12\,M_\odot$ or higher).

4 Post-formation behaviour of DNS binaries

After the DNS binary has formed the subsequent evolution will proceed as follows. As the system is spherically asymmetric in motion, it will emit gravitational waves and its orbital separation will reduce. This in turn will eventually result in the stars merging. As argued, they probably receive a natal kick which alters the system velocity, and the binary might travel away from the host galaxy or globular cluster. The merging event is thought to result in a SGRB. As will be discussed below, the demographics of DNS binaries can give hints of the occurrence of SGRB, but also vice versa.

4.1 Gravitational waves

The effect of GW emission on a binary system was predicted by Peters (1964) in terms of differential equations relating the decrease of orbital separation a and eccentricity e:

$$\frac{da}{dt} = -\frac{64G^3 m_1 m_2 (m_1+m_2)}{5a^3c^5}\frac{(1+e^2\frac{73}{24}+e^4\frac{37}{96})}{(1-e^2)^{\frac{7}{2}}}$$

and

$$\frac{de}{dt} = -\frac{304}{15}\frac{G^3}{c^5}\frac{m_1 m_2 (m_1+m_2)}{a^4}\frac{e}{(1-e^2)^{5/2}}(1+\frac{121}{304}e^2)$$

Solving for inspiral time, an analytic solution can be found in the circular case to be

$$\tau_{inspiral} = a_0^4 \frac{5}{256}\frac{c^5}{G^3}\frac{1}{m_1 m_2}\frac{1}{m_1+m_2}$$

whereas the non-circular case can be given to first order (Lorimer 2008) by:

$$\tau_{inspiral} = 10^7 yr P_{orb,h}^{8/3}(\frac{m}{M_\odot})^{-2/3}(\frac{\mu}{M_\odot})^{-1}(1-e^2)^{7/2}$$

These predictions carry important implications for our work. Inspecting the last equation it follows that an eccentric system has a quicker inspiral rate. Conversely the reverse statement also holds; that is two systems with the same characteristic age but differing in eccentricity will have had a considerable difference in initial separation and eccentricity. Although trivial, the latter statement will become more important when integrating these equations backwards in time over the binary age.

Evidence for GW was not observationally indirectly confirmed until Hulse & Taylor (1975) reported the discovery of the famous "Hulse-Taylor pulsar".

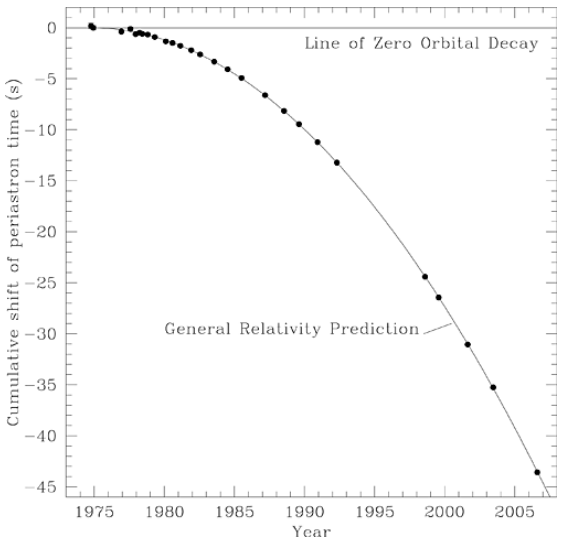

Figure 5: The observed inspiral of the famous "Hulse-Taylor pulsar". Courtesy of Lorimer (2008).

Figure 5 gives the cumulative decrease of the periastron time. Recall that $B1913$ is a rather eccentric system with $e \approx 0.6$. As the system loses angular momentum by GW emission, the orbital period will shrink. The line corresponds to this prediction by GR. As can be seen, the subsequent observations have been in very good agreement with the prediction.

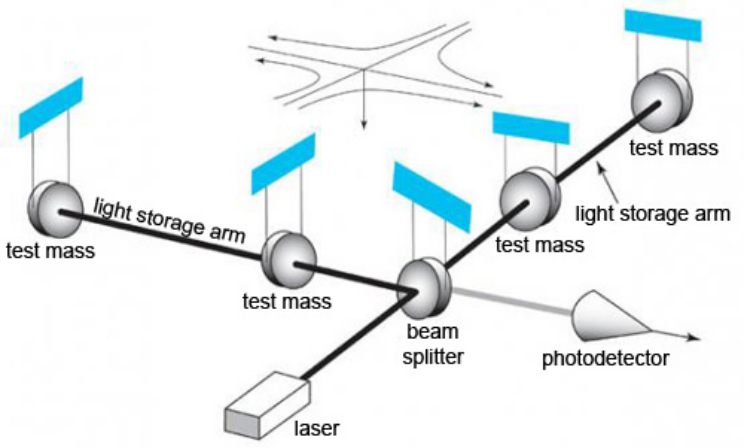

Figure 6: The interferometer setup for LIGO. Courtesy of www.ligo.org.

Currently various detectors try to detect GW directly but so far there have been no results (Abbott et al. 2010). The most sensitive detector so far is LIGO (Figure 6), but two other detectors also in action are VIRGO and GEO600. LIGO works roughly as follows: the laser sends out light to the test masses which is reflected by mirrors and the registered by the photodetector. When the gravitational wave passes by, space-time will be slightly distorted yielding a slight phase shift in the returning light. Thus one can register a gravitational wave.

It should be noted that the space-time distortion is rather small and that to register a GW would require high sensitivity. The detector sensitivity is currently increasing and it is thought that gravitationally violent events will soon be within the observational grasp. Advanced LIGO, an upgrade, will likely be operational around 2015 and it is believed that this upgrade will make the observation of events such as SGRB to be possible. Waldman (2011) estimate the likely binary coalescence detection rate to be $1 - 1000\ /yr$.

4.2 Merger rates and SGRB

Short Gamma Ray Bursts are very intense gamma ray flashes with duration less than $\sim 2\ s$, as opposed to the Long GRB that have longer durations. The difference between Short and Long GRB is, besides duration, also their demography. Whereas the LGRB are exclusively found in younger galaxies, the SGRB are found in all types of galaxies, even those where star formation has ceased. From this one would draw the conclusion that as the LGRB progenitors are likely to be connected with the death of massive stars, the SGRB progenitors involve much older objects and might be the result of the merging of compact objects.

The SGRB are related to DNS binaries from a demographic point of view. As the SGRB is believed to be a merging of a DNS binary, the merger rate would give hints of the frequency of DNS binaries. One can estimate DNS mergers mainly in two ways; either to use populations synthesis, or to extrapolate from the observed DNS binaries. Kalogera et al. (2004) estimated the DNS merger rate by extrapolating the known DNS binaries and found a merger rate of $1.7 \times 10^{-5} - 2.9 \times 10^{-4}\ yr^{-1}$ in the Milky Way. An estimate from population synthesis done by O'Shaughnessy et al. (2008) gave $3 \times 10^{-5}\ yr^{-1}$. After the second SN they system will travel along a trajectory in the galaxy and perhaps the coalescence will occur out of the galactic disc, as has been modelled e.g. by Church et al. (2011).

4.3 Spindown

For a physical quantity ϕ, its time-scale is defined as $\tau_{ts} = \frac{\phi}{\dot{\phi}}$. Analogously for rotating NS, their characteristic age τ_{char}, which is used to approximate their age, is defined as $\tau_{char} = \frac{P}{2\dot{P}}$. P denotes as usual the spin period, and the factor $1/2$ is conventional. Studying the pulsar demography for NS one finds that they are non-randomly distributed. The pulsar ages are usually of the order of $1 - 10\, GYr$, but with certain exceptions.

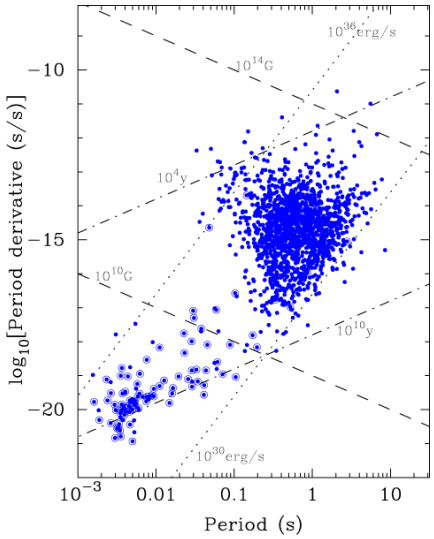

Figure 7: Plot of the currently known pulsar demography in $\log \dot{P} - P$-diagram. The dots with circles represent binaries. Courtesy of Lorimer (2008).

Note in Figure 7 above that the binaries are occur at higher rotation velocities and the singleton stars are concentrated around spins of $P \sim 1\, s$ and $\dot{P} \sim 10^{-15}\, s/s$. This should not be suprising as in the binary it is believed (Dewi & Pols 2003) that the subsequent Roche-lobe overflow will "spin up" the older pulsar and thus giving a higher rotation velocity, whereas the singleton stars are non-recycled.

Moreover, the $\dot{P} - P$ relation can be used to estimate the magnetic field of the NS. Following the dipole model, the model which is used to describe a pulsar, it can be theoretically shown that $B \propto P\dot{P}$. This relation gives typical field-strengths of order $10^7 - 10^{12}\, G$, which implies certain difficulties for the above mentioned neutrino-driven kick mechanism.

5 Some useful definitions and some pre- and post-SN relations

This section contains derivations of some mathematical formulas that will be used later in the simulations. We have as input a two-body system with given masses and separation which upon SN will have one star lose mass and receive an additional velocity, and we wish to express the change in quantities mathematically. This will be done for various quantities such as energy and angular momentum. The calculations will be based on the formalism used by Brandt & Podsiadlowski (1995).

5.1 Defining the coordinate system

As argued in above sections, the system prior to the SN event is circularized. The coordinate frame will be chosen so as to have the center of mass (CM) at the origin. The NSs will be placed on the y-axis with velocity vectors parallel and anti-parallel to the x-axis. The older pulsars is denoted m_2, the He-core m_1 and the newly formed NS $m_1\prime$. They have distances from the origin a_1 and a_2, respectively. This is depicted below.

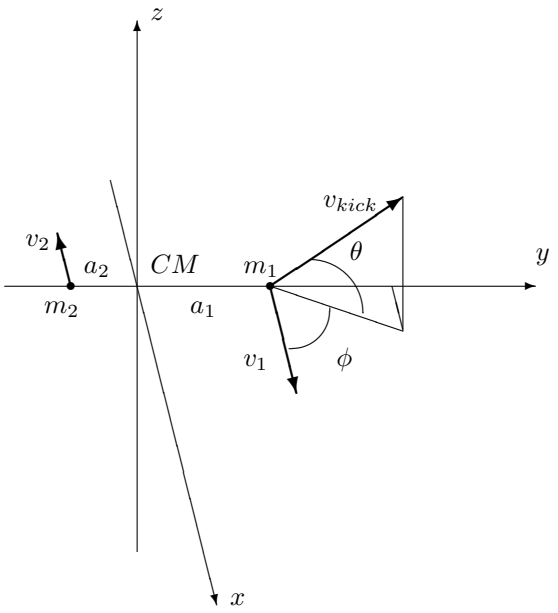

Figure 8: A geometrical picture of the framework

5.2 Definitions and some derivations of useful relations

First, for further calculation, the following definition will be useful:

$$v_{orb} = v_1 - v_2$$

and

$$\tilde{v} = \frac{|v_{kick}|}{|v_{orb}|}$$

The use for the definitions become apparent after the following calculations:

$$v_{orb}^2 = |v_1 - v_2|^2 = |v_1|^2 - 2v_1 \cdot v_2 + |v_2|^2$$

Considering the geometry of the system, the scalar product becomes the absolute values times a minus sign. Furthermore, the definition of the origin O at the CM gives the following result:

$$v_{orb}^2 = |v_1 - v_2|^2 = |v_1|^2 + |v_2|^2 + 2|v_1||v_2| = |v_1|^2(1 + \frac{a_2}{a_1})^2 = |v_1|^2(1 + \frac{m_1}{m_2})^2$$

But there is also from the force equation $F_{centrifugal} = F_{gravity}$ the relation

$$F_{centrifugal} = \frac{m_1}{a_1}v_1^2 = G\frac{m_1 m_2}{(a_1 + a_2)^2} = F_{gravity} \Leftrightarrow v_1^2 = a_1 G\frac{m_2}{(a_1 + a_2)^2}, \qquad v_1\, m_1\, a_1 \;\leftrightarrow\; v_2\, m_2\, a_2$$

This combined gives

$$v_{orb}^2 = v_1^2(1 + \frac{a_2}{a_1})^2 = G\frac{m_2}{(a_1 + a_2)^2}a_1(1 + \frac{a_1}{a_2})^2 = G\frac{m_2}{(a_1 + a_2)}(1 + \frac{m_1}{m_2}) =$$

$$= \frac{G}{(a_1 + a_2)}(m_1 + m_2) = G\frac{m_1 + m_2}{a}$$

where the relation $(1 + m_1/m_2) = (1 + a_2/a_1)$ has been used. Consider now the well-known Kepler's third law for circular orbits:

$$\frac{P^2}{a^3} = \frac{4\pi^2}{G(m_1 + m_2)}$$

with P being the binary period, and a the semi-major axis. Inserting the above result for v_{orb} gives

$$\frac{4\pi^2}{P^2} = G\frac{m_1 + m_2}{a^3} = \frac{v_{orb}^2}{a^2} \Rightarrow v_{orb}^2 = \frac{4\pi^2}{P^2}a^2 \rightarrow$$

$$\rightarrow v_{orb}^3 = \frac{8\pi^3}{P^3}a^3 = \frac{8\pi^3}{P}G\frac{m_1 + m_2}{a^3 4\pi^2}a^3 = \frac{2\pi G(m_1 + m_2)}{P}$$

5.3 Derivation of post-supernova center of mass velocity

The first star m_1 undergoes explosion and as a result loses mass and gets a kick v_{kick}. The mass loss will be denoted

$$m_1 \rightarrow m_1\prime = m_1 - \Delta m, \qquad \Delta m > 0$$

The kick vector v_{kick} will be parametrized in polar coordinates, projected along v_1, with the polar coordinate system having $\phi = 0$ along the x-axis, and $\theta \in (-\pi/2, \pi/2)$ with $\theta = 0$ in the x-y plane, just as shown in Figure 8.

As the binary undergoes the SN, the CM will get a non-trivial velocity in the labframe S. To evaluate the energy in the in the new CM-frame $S\prime$, the CM-velocity must first be calculated. The generic definition of center of mass velocity is

$$v_{CM} = \frac{\sum_i m_i v_i}{\sum_i m_i}$$

As the coordinate system were defined such that the velocities were parallel (or anti-parallel) with the x-axis, the y- and z-axes of v_{CM} will follow directly from the kick-velocity projection:

$$v_{CM,\,y} = \frac{m_1\prime}{m_1\prime + m_2}v_{kick,\,y} = \frac{m_1\prime}{m_1\prime + m_2}\tilde{v}v_{orb}\sin\phi\cos\theta$$

as $v_{kick} = \tilde{v}v_{orb}$. The z-axis has only contributions from v_{kick} and is thus given by

$$v_{CM,\,z} = \frac{m_1\prime}{m_1\prime + m_2}v_{kick,\,z} = \frac{m_1\prime}{m_1\prime + m_2}\tilde{v}v_{orb}\sin\theta$$

The x-components are somewhat more complicated, as the second star also gives a contribution.

$$v_{CM,\,x} = \frac{m_1\prime(v_1 + v_{kick,\,x}) - m_2 v_2}{m_1\prime + m_2} = \frac{m_1\prime(v_1 + \tilde{v}v_{orb}\cos\phi\cos\theta) - m_2 v_2}{m_1\prime + m_2} =$$

$$= v_{orb}\frac{m_1\prime(\frac{m_2}{m_1+m_2} + \tilde{v}\cos\phi\cos\theta) - m_2\frac{m_1}{m_1+m_2}}{m_1\prime + m_2} =$$

$$= \frac{v_{orb}}{m_1\prime + m_2}\left[\frac{m_2}{m_1+m_2}(m_1\prime - m_1) + m_1\prime\tilde{v}\cos\phi\cos\theta\right]$$

The absolute value of v_{CM} can be also be calculated:

$$|v_{CM}|^2 = v_{CM,\,x}^2 + v_{CM,\,y}^2 + v_{CM,\,z}^2 =$$

$$= (\frac{v_{orb}}{m_1\prime + m_2})^2\left[\frac{m_2}{m_1+m_2}(m_1\prime - m_1) + m_1\prime\tilde{v}\cos\phi\cos\theta\right]^2 +$$

$$+\left[\frac{m_1\prime}{m_1\prime+m_2}\tilde{v}v_{orb}\sin\phi\cos\theta\right]^2 + \left[\frac{m_1\prime}{m_1\prime+m_2}\tilde{v}v_{orb}\sin\theta\right]^2 =$$

$$= (\frac{v_{orb}}{m_1\prime + m_2})^2\left[(\frac{m_2}{m_1+m_2})^2(m_1\prime - m_1)^2 + 2\frac{m_2}{m_1+m_2}m_1\prime\tilde{v}\cos\phi\cos\theta +\right.$$

$$\left. + (m_1\prime\tilde{v}\cos\phi\cos\theta)^2 + (m_1\prime\tilde{v}\sin\phi\cos\theta)^2 + (m_1\prime\tilde{v}\sin\theta)^2\right] =$$

$$= (\frac{v_{orb}}{m_1\prime + m_2})^2\left[(\tilde{v}m_1\prime)^2 - 2\frac{\Delta m\mu m_1\prime}{m_1}\tilde{v}\cos\phi\cos\theta + (\frac{\mu\Delta m}{m_1})^2\right]$$

with the usual definitions

$$\mu \equiv \frac{m_1m_2}{m_1+m_2}, \qquad \Delta m \equiv (m_1 - m_1\prime)$$

5.4 An expression of the post-SN CM-frame energy

The new energy can in the be split up into terms of kinetic energy and a term for the potential energy. The potential energy E_{pot} is trivially given by

$$E_{pot} = -G\frac{m_1\prime m_2}{a}$$

The kinetic terms will be given after a Galilean transformation to the CM system. The general transformation is

$$v_i \rightarrow v_i\prime = v_i - v_{CM}$$

The first star velocity in the new frame will be calculated below. The y- and z-components of v_1 are all zero. Thus,

$$|v_1\prime|^2 = |v_1 + v_{kick} - v_{CM}|^2 =$$

$$= \left[v_{1,\,x} + v_{orb}\tilde{v}\cos\phi\cos\theta - \frac{v_{orb}}{m_1\prime+m_2}(\frac{m_2}{m_1+m_2}(m_1\prime - m_1) + m_1\prime\tilde{v}\cos\phi\cos\theta)\right]^2 +$$

$$+\left[\tilde{v}v_{orb}\sin\phi\cos\theta - \frac{m_1\prime}{m_1\prime+m_2}\tilde{v}v_{orb}\sin\phi\cos\theta\right]^2 + \left[\tilde{v}v_{orb}\sin\theta - \frac{m_1\prime}{m_1\prime+m_2}\tilde{v}v_{orb}\sin\theta\right]^2 =$$

$$= \left[v_{1,\,x} + \tilde{v}v_{orb}\cos\phi\cos\theta(1 - \frac{m_1\prime}{m_1\prime+m_2}) + \frac{m_2}{m_1+m_2}(\frac{m_1-m_1\prime}{m_1\prime+m_2})\right]^2 +$$

$$+\left[\tilde{v}v_{orb}\sin\phi\cos\theta(1 - \frac{m_1\prime}{m_1\prime+m_2})\right]^2 + \left[\tilde{v}v_{orb}\sin\theta(1 - \frac{m_1\prime}{m_1\prime+m_2})\right]^2$$

Now break out the v_{orb} term and use the relation $v_{orb} = v_1(1 + m_1/m_2)$.

$$\frac{|v_1\prime|}{v_{orb}^2} = \left[\frac{m_2}{m_1+m_2}\right]^2 + 2\frac{m_2}{m_1+m_2}\tilde{v}\cos\phi\cos\theta(1 - \frac{m_1\prime}{m_1\prime+m_2}) + \left[\tilde{v}\cos\phi\cos\theta(1 - \frac{m_1\prime}{m_1\prime+m_2})\right]^2 +$$

$$+2\left[(\frac{m_2}{m_1+m_2}) + \tilde{v}\cos\phi\cos\theta(1 - \frac{m_1\prime}{m_1\prime+m_2})\right]\frac{m_2}{m_1+m_2}(\frac{m_1-m_1\prime}{m_1\prime+m_2}) +$$

$$\left[\frac{m_2}{m_1+m_2}(\frac{m_1-m_1\prime}{m_1\prime+m_2})\right]^2 + \left[\tilde{v}\sin\phi\cos\theta(1 - \frac{m_1\prime}{m_1\prime+m_2})\right]^2 + \left[\tilde{v}\sin\theta(1 - \frac{m_1\prime}{m_1\prime+m_2})\right]^2 =$$

$$= \left[\tilde{v}(\frac{m_2}{m_1\prime + m_2})\right]^2 + 2\tilde{v}\cos\phi\cos\theta(\frac{m_2}{m_1\prime + m_2})\frac{m_2}{m_1 + m_2}(\frac{m_1 + m_2}{m_1\prime + m_2})+$$

$$+(\frac{m_2}{m_1 + m_2})^2\left[1 + 2\frac{m_1 - m_1\prime}{m_1\prime + m_2} + (\frac{m_1 - m_1\prime}{m_1\prime + m_2})\right]^2 =$$

$$= \left[\tilde{v}(\frac{m_2}{m_1\prime + m_2})\right]^2 + 2\tilde{v}\cos\phi\cos\theta(\frac{m_2}{m_1\prime + m_2})^2 + \left[(\frac{m_2}{m_1 + m_2})(1 + \frac{m_1 - m_1\prime}{m_1\prime + m_2})\right]^2$$

The last factor in the last term will simplify according to

$$(\frac{m_2}{m_1 + m_2})^2(1 + \frac{m_1 - m_1\prime}{m_1\prime + m_2})^2 = (\frac{m_2}{m_1 + m_2})^2(\frac{m_1 + m_2}{m_1\prime + m_2})^2 = (\frac{m_2}{m_1\prime + m_2})^2$$

The same calculation as above will be done for $v_2\prime$. Here it is simpler as the second star doesn't receive a kick. Thus, with v_2 having negative sign as above,

$$\frac{|v_2\prime|^2}{v_{orb}^2} = \left[(-v_2 - v_{CM,\,x})^2 + (-v_{CM,\,y})^2 + (-v_{CM,\,z})^2\right] =$$

$$= \left[\frac{m_1}{m_1 + m_2} + \frac{1}{m_1\prime + m_2}(\frac{m_2}{m_1 + m_2}(m_1\prime - m_1) + m_1\prime\tilde{v}\cos\phi\cos\theta)\right]^2 +$$

$$+ \left[\frac{m_1\prime}{m_1\prime + m_2}\tilde{v}\sin\phi\cos\theta\right]^2 + \left[\frac{m_1\prime}{m_1\prime + m_2}\tilde{v}\sin\theta\right]^2 =$$

$$= (\frac{m_1}{m_1 + m_2})^2 + 2\frac{m_1}{m_1 + m_2}\frac{1}{m_1\prime + m_2}\left[\frac{m_2}{m_1 + m_2}(m_1\prime - m_1) + m_1\prime\tilde{v}\cos\phi\cos\theta\right] +$$

$$+(\frac{1}{m_1\prime + m_2})^2\left[(\frac{m_2}{m_1 + m_2}(m_1\prime - m_1))^2 + 2\frac{m_1\prime m_2}{m_1 + m_2}(m_1\prime - m_1)\tilde{v}\cos\phi\cos\theta+\right.$$

$$\left.+(m_1\prime)^2\tilde{v}^2\cos^2\phi\cos^2\theta\right] + (\frac{m_1\prime}{m_1\prime + m_2})^2(\sin^2\phi\cos^2\theta + \sin^2\theta) =$$

$$= (\frac{m_1\prime}{m_1\prime + m_2})^2\tilde{v}^2(\cos^2\phi\cos^2\theta + \sin^2\theta + \sin^2\phi\cos^2\theta)+$$

$$+2\tilde{v}\cos\phi\cos\theta\left[(\frac{m_1\prime}{m_1\prime + m_2})(\frac{m_1}{m_1 + m_2}) + (\frac{m_2}{m_1 + m_2})(\frac{m_1\prime}{m_1\prime + m_2})(\frac{m_1\prime - m_1}{m_1\prime + m_2})\right] +$$

$$+(\frac{m_1}{m_1 + m_2})^2 + 2(\frac{m_1}{m_1\prime + m_2})(\frac{m_2}{m_1\prime + m_2})(\frac{m_1\prime - m_1}{m_1\prime + m_2}) + \left[(\frac{m_2}{m_1\prime + m_2})(\frac{m_1\prime - m_1}{m_1\prime + m_2})\right]^2$$

After this algebra and further simplifications, the expression becomes

$$\frac{|v_2\prime|^2}{v_{orb}^2} = \left[(\frac{m_1\prime}{m_1\prime + m_2})\tilde{v}\right]^2 + (\frac{m_1}{m_1 + m_2})^2\left[1 + 2\frac{m_2}{m_1}\frac{m_1\prime - m_2}{m_1\prime + m_2} + (\frac{m_2}{m_1}\frac{m_1\prime - m_2}{m_1\prime + m_2})^2\right] +$$

$$+2\tilde{v}^2\cos\phi\cos\theta(\frac{m_1\prime}{m_1\prime + m_2})^2 =$$

$$= \left[(\frac{m_1\prime}{m_1\prime + m_2})\tilde{v}\right]^2 + 2\tilde{v}^2\cos\phi\cos\theta(\frac{m_1\prime}{m_1\prime + m_2})^2 + (\frac{m_1}{m_1 + m_2})^2\left[1 + \frac{m_2}{m_1}(\frac{m_1\prime - m_2}{m_1\prime + m_2})\right]^2$$

Analogously as for the first velocity, the last term simplifies as

$$(\frac{m_1}{m_1 + m_2})^2\left[1 + \frac{m_2}{m_1}\frac{m_1\prime - m_2}{m_1\prime + m_2}\right]^2 = (\frac{m_1}{m_1 + m_2})^2\left[\frac{m_1(m_1\prime + m_2) + m_2(m_1\prime - m_1)}{m_1(m_1\prime + m_2)}\right]^2 =$$

$$= (\frac{m_1}{m_1 + m_2})^2\left[\frac{m_1\prime(m_1 + m_2)}{m_1(m_1\prime + m_2)}\right]^2 = (\frac{m_1\prime}{m_1\prime + m_2})^2$$

Now from section 2 there is the expression for v_{orb}^2. The total kinetic energy becomes

$$E_{kin}\prime = \frac{m_1\prime}{2}|v_1\prime|^2 + \frac{m_2}{2}|v_2\prime|^2 =$$

$$= \frac{v_{orb}^2}{2} m_{1\prime} \left[\tilde{v}^2 (\frac{m_2}{m_{1\prime}+m_2})^2 + (\frac{m_2}{m_{1\prime}+m_2})^2 + 2\tilde{v}\cos\phi\cos\theta(\frac{m_2}{m_{1\prime}+m_2})^2 \right] +$$

$$+ \frac{v_{orb}^2}{2} m_2 \left[(\frac{m_{1\prime}}{m_{1\prime}+m_2})^2 \tilde{v}^2 + 2\tilde{v}^2\cos\phi\cos\theta(\frac{m_{1\prime}}{m_{1\prime}+m_2})^2 + (\frac{m_{1\prime}}{m_{1\prime}+m_2})^2 \right] =$$

$$= \frac{v_{orb}^2}{2}(1 + 2\tilde{v}\cos\phi\cos\theta + \tilde{v}^2) \left[m_2 (\frac{m_{1\prime}}{m_{1\prime}+m_2})^2 + m_{1\prime}(\frac{m_2}{m_{1\prime}+m_2})^2 \right] =$$

$$= \frac{v_{orb}}{2}(1 + 2\tilde{v}\cos\phi\cos\theta + \tilde{v}^2) \left[\frac{m_{1\prime}m_2}{(m_{1\prime}+m_2)^2}(m_{1\prime}+m_2) \right] =$$

$$= \frac{v_{orb}}{2}(1 + 2\tilde{v}\cos\phi\cos\theta + \tilde{v}^2)\frac{m_{1\prime}m_2}{(m_{1\prime}+m_2)}$$

In earlier sections, it was shown that

$$v_{orb}^2 = G\frac{m_1 + m_2}{a}$$

and that the potential component $E_{pot\prime}$ was the same except for the change in m_1. The total energy $E_{tot\prime}$ can be thus written in neat form:

$$E_{tot\prime} = -G\frac{m_{1\prime}m_2}{a} + \frac{v_{orb}}{2}(1 + 2\tilde{v}\cos\phi\cos\theta + \tilde{v}^2)\frac{m_{1\prime}m_2}{(m_{1\prime}+m_2)} =$$

$$-G\frac{m_{1\prime}m_2}{a} + G\frac{m_1+m_2}{2a}(1 + 2\tilde{v}\cos\phi\cos\theta + \tilde{v}^2)\frac{m_{1\prime}m_2}{(m_{1\prime}+m_2)} =$$

$$= -G\frac{m_{1\prime}m_2}{2a}\left[2 - \tilde{m}(1 + 2\tilde{v}\cos\phi\cos\theta + \tilde{v}^2)\right], \qquad \tilde{m} = \frac{m_1+m_2}{m_{1\prime}+m_2}$$

5.5 The relation between pre- and post-SN orbit angular momentum

L is defined as usual by $L \equiv r \times p$. In the pre-SN system, as the orbits were assumed to be circular, the vectors r and p are orthogonal giving straight-forward calculations. With the system as in the previous sections, L is trivially given by

$$L = L_1 + L_2 = r_1 \times p_1 + r_2 \times p_2 = (a_1 m_1 v_1 + a_2 m_2 v_2)e_z$$

with absolute value squared given by

$$\frac{|L|^2}{v_{orb}^2} = (a_1 m_1 v_1 + a_2 m_2 v_2)^2 = (a_1 + a_2)^2 (\frac{m_1 m_2}{m_1 + m_2})^2$$

As the system undergoes supernova the momenta will change as in previous sections. The second star does not undergo a SN and its angular momentum is thus unchanged, up to Galilean transformation. Define $L\prime$ to be the post supernova angular momentum in the new frame of rest, that is the angular momentum evaluated after having done a Galilean transformation with the v_{CM} calculated in previous sections. The following calculations yield $L\prime$.

$$L \to L\prime = L_{1\prime} + \hat{L_{2\prime}} = r_1 \times m_{1\prime}(v_1 + v_{kick} - v_{CM}) + r_2 \times m_2(v_2 - v_{CM})$$

As $v_{kick,y} || r_1$ the y-component of v_{kick} does not contribute to $L\prime$. Also, for the second star, v_{CM} has negative sign because of the definition of angular momentum. Thus,

$$L\prime = r_1 \times m_{1\prime}(v_1 + v_{kick,x}) + r_2 \times m_2(v_2 + v_{CM}) =$$

$$= \left[m_{1\prime}a_1(v_{orb}\tilde{v}\sin\theta - v_{orb}\tilde{v}\frac{m_{1\prime}}{m_{1\prime}+m_2}\sin\theta) + m_2 a_2 v_{orb}\tilde{v}\sin\theta \right] e_x +$$

$$+ a_1 m_{1\prime}\left[v_1 + v_{kick}\cos\phi\cos\theta - \frac{v_{orb}}{m_1+m_2}(\frac{m_2}{m_1+m_2}(m_{1\prime}-m_1) + m_{1\prime}\tilde{v}\cos\phi\cos\theta) \right] e_z +$$

$$a_2 m_2 \left[v_2 + \frac{v_{orb}}{m_1+m_2}(\frac{m_2}{m_1+m_2}(m_{1\prime}-m_1) + m_{1\prime}\tilde{v}\cos\phi\cos\theta) \right] e_z =$$

$$= \tilde{v} v_{orb} \sin\theta (\frac{m_1\prime}{m_1\prime + m_2}) \left[(m_2 a_2 - m_1\prime a_1) + m_1\prime a_1 \right] e_x +$$

$$+ \left[m_1\prime a_1 v_{orb} \frac{m_1}{m_1 + m_2} + m_1\prime a_1 v_{orb} \tilde{v} \cos\phi \cos\theta + m_2 a_2 v_{orb} \frac{m_1}{m_1 + m_2} \right] e_z +$$

$$+ (m_1\prime a_1 + m_2 a_2) \frac{v_{orb}}{m_1 + m_2} \left[\frac{m_2}{m_1 + m_2} (m_1\prime - m_1) + m_1\prime \tilde{v} \cos\phi \cos\theta \right] e_z$$

This can be simplified accordingly:

$$L\prime = \tilde{v} v_{orb} \sin\theta (\frac{m_1\prime}{m_1\prime + m_2}) \left[(m_2 a_2 - m_1\prime a_1) + m_1\prime a_1 (m_1\prime + m_2) \right] e_x +$$

$$\left[a_1 \frac{m_1\prime m_2}{m_1 + m_2} - (\frac{m_1\prime}{m_1\prime + m_2}) a_1 (\frac{m_2}{m_1 + m_2})(m_1\prime - m_1) + m_2 a_2 (\frac{m_1}{m_1 + m_2}) + \right.$$

$$\left. + m_2 a_2 (\frac{m_1\prime - m_1}{m_1\prime + m_2})(\frac{m_2}{m_1 + m_2}) \right] e_z +$$

$$+ \tilde{v} \cos\phi \cos\theta \left[m_1\prime a_1 - (\frac{m_1\prime}{m_1\prime + m_2}) m_1\prime a_1 + m_2 a_2 (\frac{m_1\prime}{m_1\prime + m_2}) \right] e_z =$$

$$= \tilde{v} v_{orb} \sin\theta (\frac{m_1\prime m_2}{m_1\prime + m_2})(a_1 + a_2) e_x +$$

$$+ \left[a_1 \frac{m_1\prime m_2}{m_1 + m_2} - a_1 (\frac{m_1\prime}{m_1\prime + m_2})(\frac{m_2}{m_1 + m_2})(m_1\prime - m_1) + \right.$$

$$\left. + a_2 m_2 (\frac{m_1}{m_1 + m_2}) + a_2 m_2 (\frac{m_1\prime - m_1}{m_1\prime + m_2})(\frac{m_2}{m_1 + m_2}) \right] e_z +$$

$$+ \tilde{v} \cos\phi \cos\theta (\frac{m_1\prime}{m_1\prime + m_2}) [a_1 m_1\prime + a_1 m_2 - m_1\prime a_1 + m_2 a_2] e_z +$$

Now simplify the factors individually. The factor of the term with $\tilde{v} \cos\phi \cos\theta$ becomes

$$\tilde{v} \cos\phi \cos\theta (\frac{m_1\prime}{m_1\prime + m_2})(a_1 m_2 + m_2 a_2) = \tilde{v} \cos\phi \cos\theta (\frac{m_1\prime m_2}{m_1\prime + m_2})(a_1 + a_2)$$

The second term requires a bit more work;

$$a_1 \left[\frac{m_1\prime m_2}{m_1 + m_2} - (\frac{m_1\prime}{m_1\prime + m_2})(\frac{m_2}{m_1 + m_2})(m_1\prime - m_1) \right] +$$

$$+ a_2 \left[(\frac{m_1 m_2}{m_1 + m_2}) + m_2 (\frac{m_1\prime - m_1}{m_1\prime + m_2})(\frac{m_2}{m_1 + m_2}) \right] =$$

$$= a_1 (\frac{m_1\prime}{m_1\prime + m_2})(\frac{m_2}{m_1 + m_2}) \left[(m_1\prime + m_2) - (m_1\prime - m_1) \right] +$$

$$+ a_2 (\frac{1}{m_1\prime + m_2})(\frac{m_2}{m_1 + m_2}) \left[m_1 (m_1\prime + m_2) + m_2 (m_1\prime - m_1) \right] =$$

$$= \frac{m_1\prime m_2}{m_1\prime + m_2} (a_1 + a_2)$$

Now there is a common term which can be taken out, and the resulting expression for the $L\prime$ becomes

$$L\prime = \frac{m_1\prime m_2}{m_1\prime + m_2} (a_1 + a_2) v_{orb} [(\tilde{v} \sin\theta) e_x + (1 + \tilde{v} \cos\phi \cos\theta) e_z]$$

The angle ν between the initial and final angular momentum vectors can now be calculated using the ordinary Euclidian scalar product. Observe that as the initial angular momentum vector L is parallel to the z-axis, the final angular momentum $L\prime$ can be split up in x- and a z-components, where the former is orthogonal to the L and thus does not contribute to the scalar product. The angle is thus given by

$$\cos\nu = \frac{L \cdot L_z\prime}{|L||L\prime|}$$

Thus, calculate first the above scalar product:

$$L \cdot L_{z\prime} = (a_1 m_1 v_1 + a_2 m_2 v_2) e_z \cdot \frac{m_{1\prime} m_2}{m_{1\prime} + m_2}(a_1 + a_2) v_{orb}(1 + \tilde{v}\cos\phi\cos\theta) e_z =$$

$$v_{orb}^2 \frac{m_1 m_2}{m_1 + m_2}(a_1 + a_2)\frac{m_{1\prime} m_2}{m_{1\prime} + m_2}(a_1 + a_2)(1 + \tilde{v}\cos\phi\cos\theta)$$

From the above calculated absolute value of L and taking the absolute value of $L\prime$, the angle ν is now given by

$$\cos\nu = \frac{L \cdot L_{z\prime}}{|L||L\prime|} = \frac{1 + \tilde{v}\cos\phi\cos\theta}{\sqrt{(\tilde{v}\sin\theta)^2 + (1 + \tilde{v}\cos\phi\cos\theta)^2}}$$

5.6 Post-supernova eccentricity

It can be shown from Classical Mechanics that the eccentricity e of a Newtonian potential orbit follows

$$e^2 = 1 + \frac{2EL^2(m_1 + m_2)}{G^2 m_1^3 m_2^3}$$

where L being $|L|$. For the post-supernova case and with the above expressions for energy $E\prime$ and angular momentum $L\prime$, the eccentricity becomes

$$e^2 = 1 + \frac{2E\prime L\prime^2(m_{1\prime} + m_2)}{G^2 m_{1\prime}{}^3 m_2^3} =$$

$$= 1 - \frac{2G\frac{m_{1\prime} m_2}{2a}(2 - \tilde{m}(1 + 2\tilde{v}\cos\phi\cos\theta + \tilde{v}^2))(\frac{m_{1\prime} m_2}{m_{1\prime} + m_2}(a_1 + a_2)v_{orb})^2}{G^2 m_{1\prime}{}^3 m_2^3} \times$$

$$\times \frac{[(\tilde{v}\sin\theta)^2 + (1 + \tilde{v}\cos\phi\cos\theta)^2](m_{1\prime} + m_2)}{G^2 m_{1\prime}{}^3 m_2^3} =$$

$$= 1 - \frac{aG\frac{m_1 + m_2}{a}}{G(m_{1\prime} + m_2)}(2 - \tilde{m}(1 + 2\tilde{v}\cos\phi\cos\theta + \tilde{v}^2))[(\tilde{v}\sin\theta)^2 + (1 + \tilde{v}\cos\phi\cos\theta)^2] =$$

$$= 1 - \tilde{m}(2 - \tilde{m}(1 + 2\tilde{v}\cos\phi\cos\theta + \tilde{v}^2))[(\tilde{v}\sin\theta)^2 + (1 + \tilde{v}\cos\phi\cos\theta)^2]$$

where the relation $v_{orb}^2 = G\frac{m_1 + m_2}{a}$ was used.

5.7 Some equations for the bound post-supernova system

Generally if a classical system is to be bound, it has to have $E_{tot} < 0$. This condition can easily extract bounds from the total energy in the CM-system, calculated in previous sections

$$E_{tot\prime} = -G\frac{m_{1\prime} m_2}{2a}(2 - \tilde{m}(1 + 2\tilde{v}\cos\phi\cos\theta + \tilde{v}^2))$$

Putting this negative, or said differently, putting the right product positive, gives

$$0 < (2 - \tilde{m}(1 + 2\tilde{v}\cos\phi\cos\theta + \tilde{v}^2)) \Leftrightarrow 1 + 2\tilde{v}\cos\phi\cos\theta + \tilde{v}^2 < \frac{2}{\tilde{m}} \Leftrightarrow$$

$$\Leftrightarrow \cos\phi\cos\theta < \frac{1}{2\tilde{v}}(\frac{2}{\tilde{m}} - 1 - \tilde{v}^2)$$

Furthermore, assuming spherical symmetry in randomizing ϕ and θ, the following probability can easily be shown:

$$P(\cos\phi\cos\theta < A) = \frac{1}{2}(1 + A), \qquad -1 < A < 1$$

Combining this and the inequality requirement above for a bound post SN system gives

$$P_{bound} = \frac{1}{2}(1 + \frac{1}{2\tilde{v}}(\frac{2}{\tilde{m}} - 1 - \tilde{v}^2))$$

Furthermore, there can be put constraints on $\tilde{v}$ if the post-SN system is to be bound. Denote the upper bound $\tilde{v}_{max}$. This $\tilde{v}_{max}$ is, of course, when the kick-direction is anti-parallel from v_1. This gives

$\cos\phi\cos\theta = -1$. The maximum $\tilde{v}_{max}$ occurs precisely when $E\prime = 0$. Thus it follows, from the energy formula derived above, that

$$0 = E\prime = -G\frac{m_1\prime m_2}{2a}[2 - \tilde{m}(1 - 2\tilde{v}_{max} + \tilde{v}_{max}^2)] \Leftrightarrow 2 = \tilde{m}[1 - \tilde{v}]^2$$

$$\rightarrow \tilde{v}_{max} = 1 \pm \sqrt{\frac{2}{\tilde{m}}}$$

with the plus sign corresponding to the maximum.

Another constraint can be found in the special case of $\tilde{m} > 2$. In this case a very low v_{kick} would perhaps not result in a bound system, and thus there must be a minimum $v_{kick,min}$ for which the system remains bound. It is geometrically clear that this minimum would have to occur when the kick velocity v_{kick} is anti-parallel to the initial v_1. Imitating the previous calculation it follows that this minimum is attained with the corresponding minus sign (as $1 - \sqrt{2/\tilde{m}}$ is now positive, and thus an allowed root), accordingly:

$$v_{kick,min} = 1 - \sqrt{\frac{2}{\tilde{m}}}$$

6 Constraining kicks from known DNS binaries

This section presents some of the first results. The results are some constraints on the kicks given by examining the existing DNS binary population.

The section begins with giving the "pre-requisite" values needed to simulate, that is the constraints on the progenitors. Later an example binary is studied, namely the well-known binary $J0737$. The results are discussed and some plots are presented.

After this is presented similar results for other DNS systems, gained through analogous analysis.

6.1 Constraining the progenitors of existing DNS binaries

From Table 1 in the introductory section, one can take values of existing DNS binaries and use these to put constraints on the progenitor systems. There are many degrees of freedom determining the final state, and of course, different combinations of these might give the same post-SN parameters. To get a good idea of the kick a very natural idea is thus to simulate all over the allowed progenitor phase space. This is in fact easier than it would appear as many of the pre- vs. post-SN relations are monotonic. That is, having the "corners" of the allowed phase space, it suffices to simulate these, as any post-SN parameter value would lie between the resulting "corner"-values.

So, to study the allowed kicks, one must thus first understand what possible progenitors phase space there is. As mentioned in previous sections, there is a fixed He-core mass range of $2.1 - 8\ M_\odot$ that give rise to NSs with the lower-mass progenitors yielding a white dwarf, and the higher-mass progenitors yielding a black hole. Furthermore, it is believed that the systems with He-core masses above $6.5\ M_\odot$ will undergo unstable Roche-lobe overflow and merge. One can also constrain the separation; consider a circularized binary progenitor with semi-major axis a and the massive companion going SN. At the time of SN, the then separation has to correspond to a point on the post-SN trajectory. That is, a can be at most the apastron of the post-SN system, and at least the periastron. Thus, the post-SN system has to obey the following constraint:

$$a\prime(1 - e\prime) \leq a \leq a\prime(1 + e\prime)$$

where a denotes the pre-SN system semi-major axis and $a\prime$ that of the post-SN system.[1] With this constraint on the progenitor semi-major axis, one can obtain an upper bound on the allowed mass by demanding that the He-core does not fill its Roche-lobe. To follow this argument, one of course needs to know the radius of the He-core as a function of mass, which is rather a non-trivial matter.

Finally, by considering the age of the system, one must take into account the inspiral due to gravitational wave emission and that the currently observed values of $a\prime$ and $e\prime$ have been reduced by this.

6.2 Description of simulation methodology for the kick-constraints

Having understood the above problematics, we can now now consider simulation methodology. This is done by assuming the above mass range for the progenitors, combined with them not filling their Roche-lobe. To investigate whether the He-cores fill their Roche-lobes we use a radial formula given by Tauris & van den Heuvel (2003), which is

$$R_{He} = 0.212(\frac{M_{He}}{M_\odot})^{0.654} R_\odot$$

. Initially however, another formula was used, given in Fryer & Kalogera (1997):

$$\log(R_{He}) = \begin{cases} 3.0965 - 2.013\log(M_{He}), & M_{He} < 2.5\ M_\odot \\ 0.0557(\log(M_{He}) - 0.172)^{-2.5} & M_{He} > 2.5\ M_\odot \end{cases}$$

[1] For a more "mathematical" derivation than the above intuitive one, see e.g. Flannery & van den Heuvel (1975)

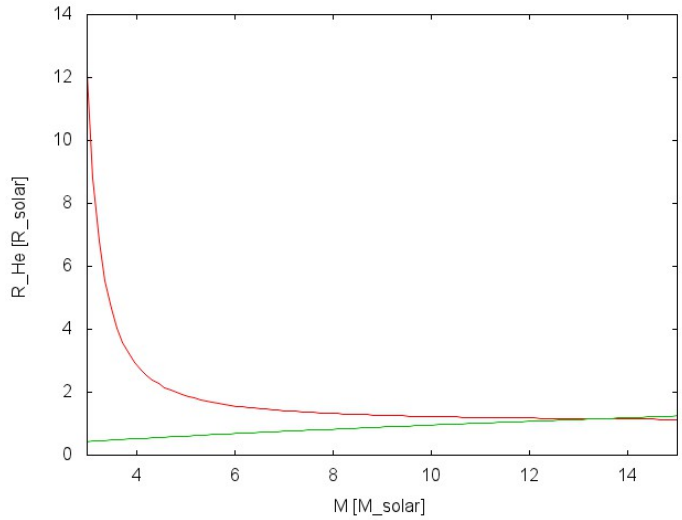

Figure 9: Plotted radial functions of the He-core. The red function is the formula given in Fryer & Kalogera (1997) whereas the green one is that of Tauris & van den Heuvel (2003).

When using the Roche-lobe formalism in Eggleton (1983), it follows from Figure 9 that the minimum separations correspond to twice that of the widest $J0737$ bound if the latter radial function is used and thus this formula was discarded.

As mentioned above, the functions relating the pre- and post-SN event are continuous and monotonic and this means that taking the "extrema" is sufficient to constrain the kicks. For each of these extrema we model some number of SNs with randomized values of θ, ϕ and v_{kick}. Following the pre- and post-SN relations derived in Section 5, the program *StarSim.java* decides whether it is bound or not and in the case of it being bound, whether it is "close" to the desired system or not. This latter condition is determined only by the post-SN eccentricity and separation in terms of $|a\prime - a_{sys}| < \epsilon_a$ and $|e\prime - e_{sys}| < \epsilon_e$.

As many systems exhibit similar properties, the above procedure is applied to some systems with varied observed properties (e.g. similar separation but varying eccentricity and vice versa).

6.3 Inspiral integration

Using a simple solver program the current system parameters can be integrated backwards in time over their characteristic age. Note that in the case of the very eccentric system $J1811-1736$ the initial separation and eccentricity corresponds in practice to an unbound system and this result is thus not possible to use. It is important to stress here the approximative nature of likening τ_c to the true age of the system, as it is in the above case much younger. We recall that the characteristic age is merely a probable true age of the system.

Table 2: Table values of current DNS binaries after integrating the GW emission.

Designation	$a\,[R_\odot]$	e
J0737-3039	1.438	0.104
B1534+12	3.410	0.288
B1913+16	3.288	0.666
J1811-1736	21877	0.999
J1756-2251	2.86	0.197

6.4 The Roche-lobe constraint

From the Table 1, J0737 has $a\prime \approx 1.290\ R_\odot$ and $e = 0.088$, which, not taking inspiral into account, gives the bound

$$1.177\ R_\odot \leq a \leq 1.403\ R_\odot$$

for the progenitor system.

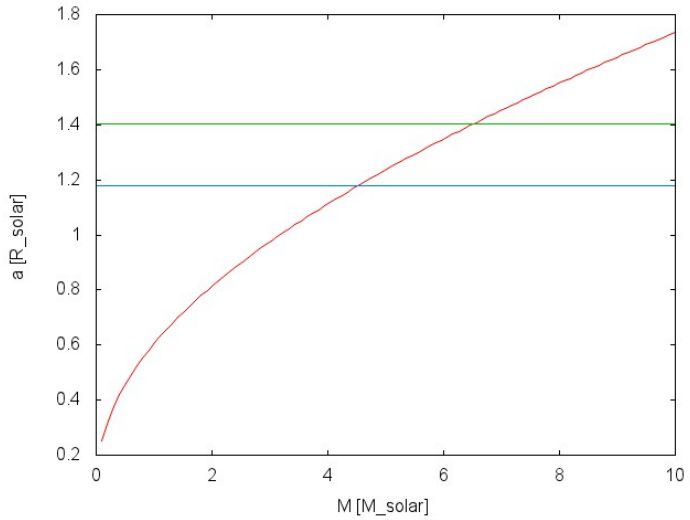

Figure 10: Plotted radial functions $R_{He}(M_{He})/f(q)$ with $f(q)$ being the usual Eggleton quote and the radial function taken to be that of Tauris & van den Heuvel (2003). The red line corresponds to the minimum separation for the system not to fill its Roche-lobe. The two straight lines are those of $a\prime(1-e\prime) = 1.177\ R_\odot$ and $a\prime(1+e\prime) = 1.404\ R_\odot$. Intersections correspond to $4.5\ M_\odot$ and $6.5\ M_\odot$

In Figure 10 we see the intersections corresponding to $m_1 = 4.5\ M_\odot$ and $m_1 = 6.5\ M_\odot$. Thus, the above constraints give rise to a bounded allowed subset of the phase space consisting of the pairs (m_1, a), with "corners" in $(2.1\ M_\odot, 1.177\ R_\odot)$, $(2.1\ M_\odot, 1.404\ R_\odot)$, $(4.5\ M_\odot, 1.177\ R_\odot)$ and $(6.5\ M_\odot, 1.404\ R_\odot)$ where we recall that $2.1\ M_\odot$ is the lowest He-core mass which is believed to yield a NS remnant.

6.5 Simulating the $J0737$ phase space

For $J0737$ the system is very special. It is the tightest of the binaries and it has a very low eccentricity, which has yielded very useful constraints. With the above constraints on phase-space we conducted the below plots. The remnant masses were taken from Table 1, with $m_1 = 1.25\ M_\odot$ and $m_2 = 1.34\ M_\odot$.

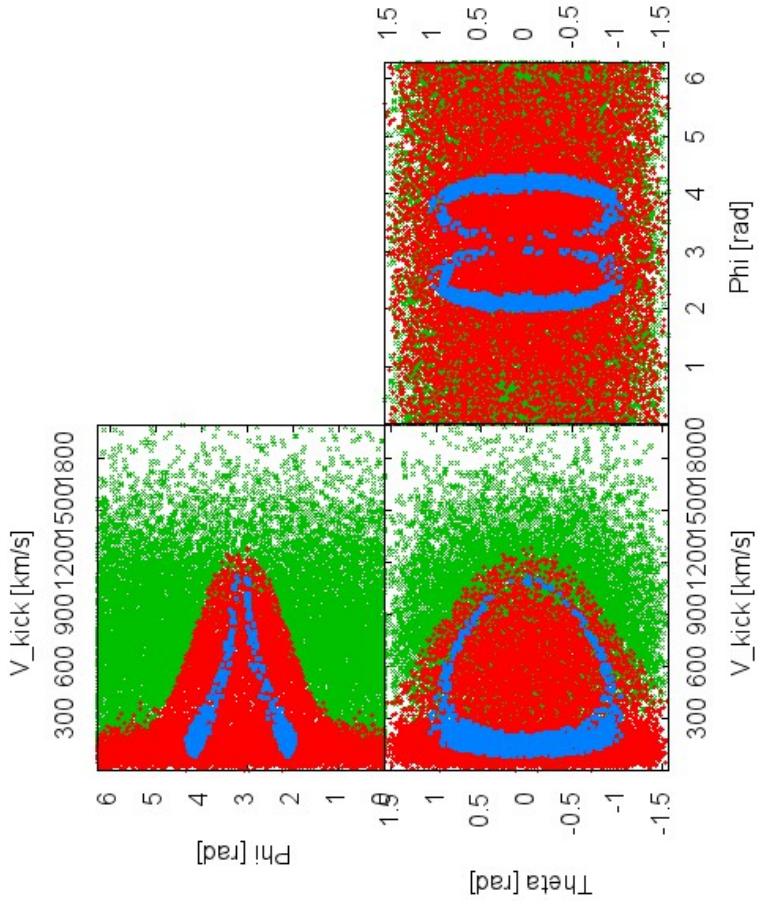

Figure 11: Plot of the progenitor system of *J0737* with $a = 1.18\,R_\odot$ and $m_1 = 2.1\,M_\odot$. Green plots are the unbound systems, the red plots are the bound ones and the blue plots are close to *J0737* with $|e\prime - e_{J0737}| < 0.05$ and $|a\prime - a_{J0737}| < 0.1$.

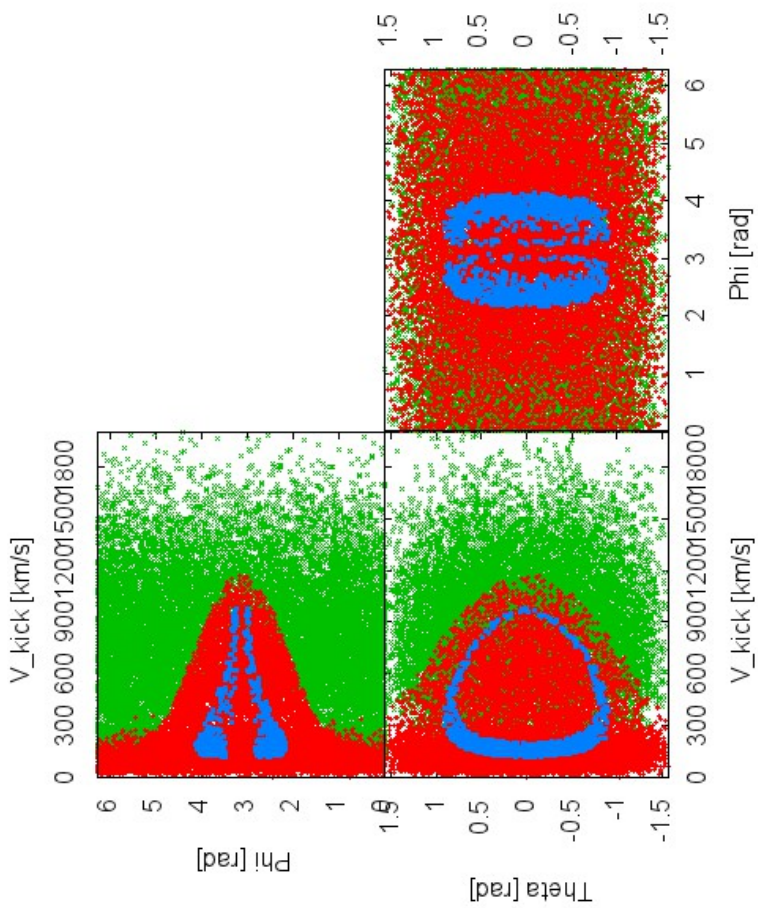

Figure 12: Plot of the progenitor system of *J0737* with $a = 1.40\ R_\odot$ and $m_1 = 2.1\ M_\odot$. Green plots are the unbound systems, the red plots are the bound ones and the blue plots are close to *J0737* with $|e\prime - e_{J0737}| < 0.05$ and $|a\prime - a_{J0737}| < 0.1$.

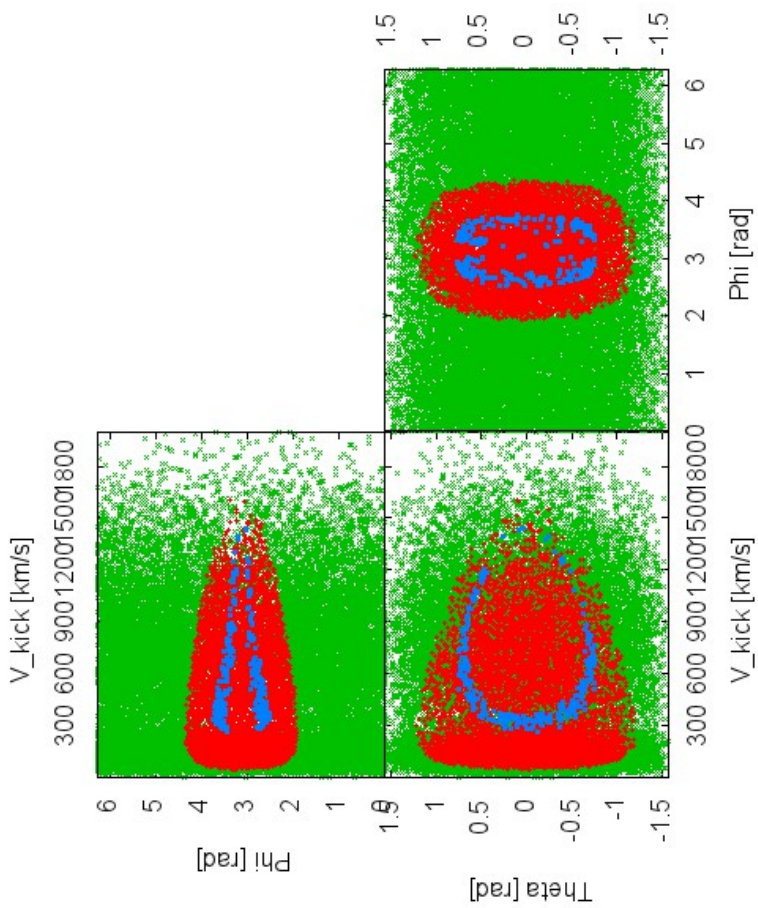

Figure 13: Plot of the progenitor system of *J0737* with $a = 1.18\,R_\odot$ and $m_1 = 4.5\,M_\odot$. Green plots are the unbound systems, the red plots are the bound ones and the blue plots are close to *J0737* with $|e\prime - e_{J0737}| < 0.05$ and $|a\prime - a_{J0737}| < 0.1$.

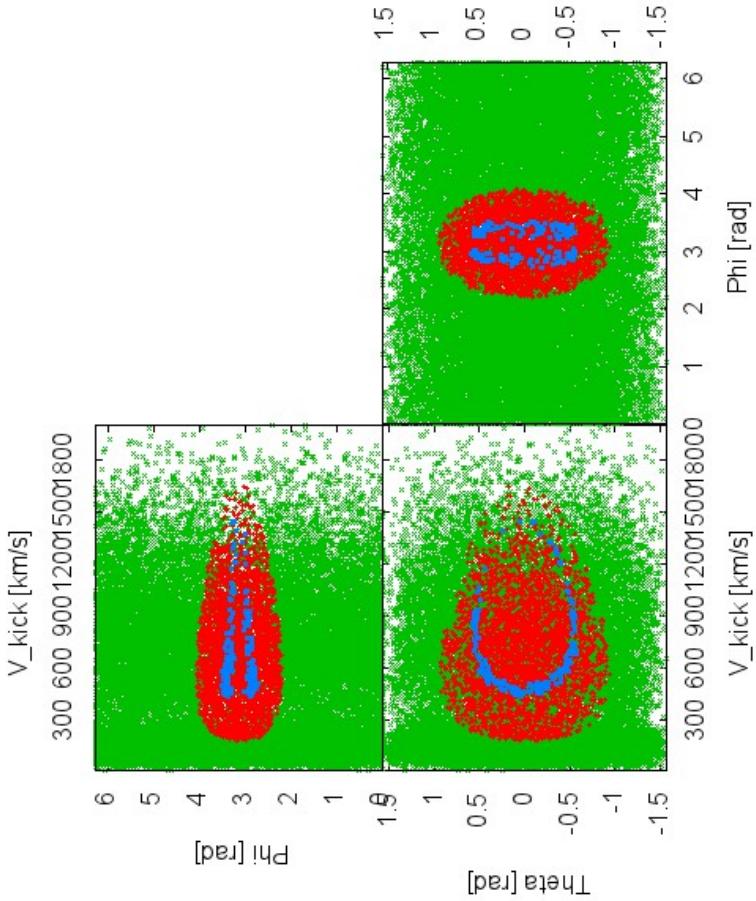

Figure 14: Plot of the progenitor system of *J0737* with $a = 1.40\ R_\odot$ and $m_1 = 6.5\ M_\odot$. Green plots are the unbound systems, the red plots are the bound ones and the blue plots are close to *J0737* with $|e\prime - e_{J0737}| < 0.05$ and $|a\prime - a_{J0737}| < 0.1$.

6.5.1 The plots and their implications

As can be seen, the constraints on ϕ and θ are rather strong, in particular for ϕ which has to be directed so as to be very anti-parallel. Furthermore the plots are clear concerning θ; there cannot have been a polar kick, as speculated by Willems et al. (2008). In the two first cases, that is with $m_1 = 2.1\,M_\odot$, low kicked stars remain bound. This is of course consistent with the mathematics, which states that $v_{kick,min}$ only exists when $\tilde{m} > 2$, as is not the case with this mass. For the latter two plots this is the case and consequently they can not have had lower velocity kicks. These examples are very interesting taking into account the spin-period eccentricity relation described in above sections, stating a PDF with with low dispersion. Such a kick magnitude would not have resulted in a bound system, implying that either the upper masses is not a possible progenitor or that the system did not follow the low kick magnitude distribution. The main observation is hence that the SN must have been asymmetric.

The "bifurcation" that is visible in the v_{kick}-ϕ diagram can at first sight appear surprising. The simulations where redone with loosened constraints and as a result the "bifurcations" disappeared, whereas for strong enough constraints there could be no "close" systems with $\phi = \pi$. The phenomenon might not be too surprising; one could argue that given a fixed kick angle (that is fixed θ and ϕ), there are two parameters to fix "close" to the sought for post-SN parameters ($a\prime$ and $e\prime$), but only one degree of freedom with $\tilde{v}$. Thus, to fix $a\prime$ within the "close" range, there is by continuity of the eccentricity equation only a limited allowed range of $\tilde{v}$ and this range does not necessarily correspond to the corresponding range of "close" $e\prime$. This can be seen mathematically; Taking the equations from Section 5 for eccentricity and energy and fixing $\phi = \pi$ as in a anti-parallel kick one gets

$$\frac{a}{a\prime} = 2 - \tilde{m}(1 - 2\tilde{v}\cos(\theta) + \tilde{v}^2)$$

and

$$e^2 = 1 - \tilde{m}(2 - \tilde{m}(1 - 2\tilde{v}\cos(\theta) + \tilde{v}^2))(\tilde{v}^2\sin^2(\theta) + (1 - \tilde{v}\cos(\theta))^2)$$

with parameters from e.g. case one in the $J0737$ situation the values are $a/a\prime \approx 1.088$ and $e^2 = 0.007744$. These equations can now be equated to form a new function F of the two variables $\tilde{v}$ and θ, with the corresponding post-SN parameters corresponding to $F = 0$.

$$F = -\frac{a}{a\prime} + 2 - \tilde{m}(1 - 2\tilde{v}\cos(\theta) + \tilde{v}^2) -$$

$$-e^2 + 1 - \tilde{m}(2 - \tilde{m}(1 - 2\tilde{v}\cos(\theta) + \tilde{v}^2))(\tilde{v}^2\sin^2(\theta) + (1 - \tilde{v}\cos(\theta))^2)$$

This function is graphed in Figure 15.

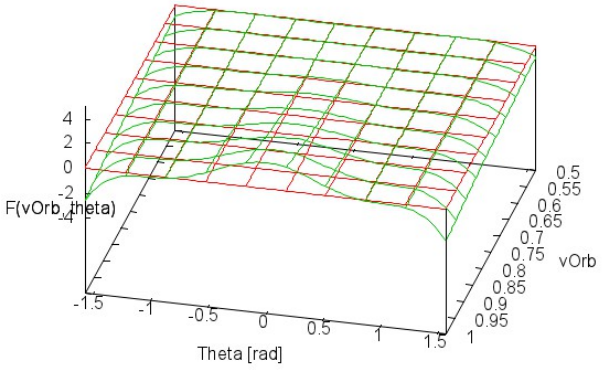

Figure 15: Plotting the above defined function $F(\tilde{v}, \theta)$ and a constant plane at $z = 0$. The intersection corresponds to allowed solutions for the kick to be considered "close".

As can be seen, $F = 0$ corresponds to a rather polarly inclined kick. In the above plots, the high velocity kicks are the ones corresponding to the wider θ, which is precisely what this plot says; a planar ($\theta = 0$) kick would correspond to low kick velocities, and there there can be no solution.

The v_{kick}-θ have its bound systems forming a "ring" in the plot. The same explanation as above holds also here. The limited degrees of freedom only allow for certain solutions for a sufficient constraint on the post-SN parameters.

We also comment on the fact that in certain systems the plots show a "false" $v_{kick,max}$, meaning that the true maximum kick velocity in fact supercedes that of the highest plotted bound kicked system. The reason is merely due to probability; a high-kick bound system is much more unlikely.

6.5.2 The role of the system age

One must know the difference between the current data and the implications of the data integrated backwards in time. Using the same methods by Roche-lobe constraints we found, after integrating *J0737* back in time over its characteristic age τ_c, the separation and eccentricity. These are stated in Table 2. The progenitor separation range in this case is $1.29 \leq a \leq 1.59$. This yields for the above mass in the case of $a = 1.29\, R_\odot$ a maximum of $5.5\, M_\odot$ from the Roche-lobe contraint.

Comparing the phase space point of $(1.18\, R_\odot, 2.1\, R_\odot)$ to the same corresponding point one finds the result in the below plot:

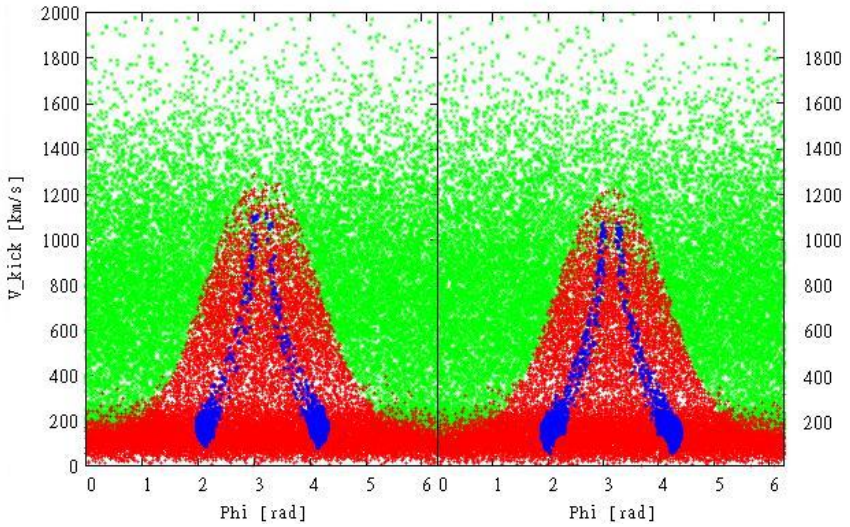

Figure 16: Comparison of the plots with the lowest allowed mass and lowest allowed separation for the available data of *J0737* with and without having integrated back along the systems characteristic age τ_c. The right plot has values after backwards integration.

As can be seen in Figure 16, the difference is negligible. The same result is, of course, obtained when investigating the other extrema, with maximum separation and masses, as depicted below. The result is hardly surprising as one could already have seen in the previous plots, where the difference between maximum and minimum separation was very small.

The one noticeable difference is the slightly lowered allowed range for the systems to remain "close". It can be explained by considering the difference generically; as the system is integrated backwards it has a wider orbit. This in turn, leads to v_{orb} getting lower. If the system is to retain its separation there is in the wider orbit now a lower requirement of v_{kick} so as to compensate for the mass loss. Conversely the same argument holds when considering the maximum for the system to be "close".

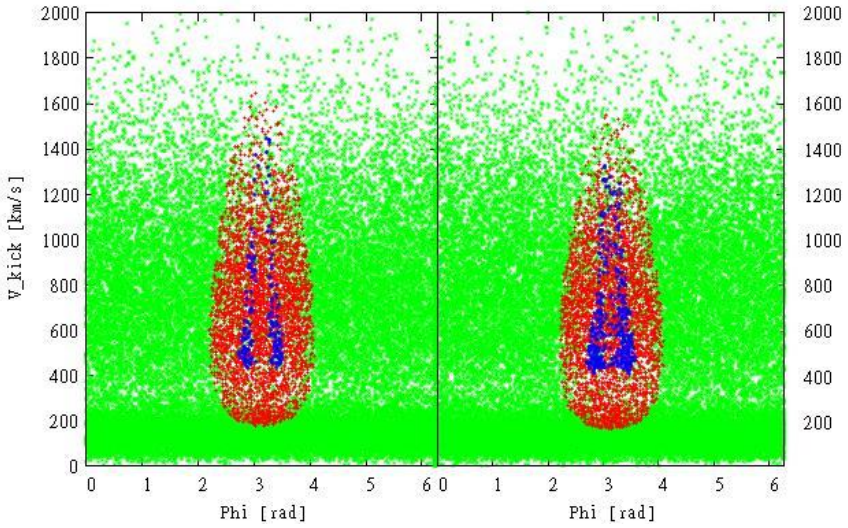

Figure 17: Comparison of the plots with the maximum allowed mass and maximum allowed separation for the available data of $J0737$ with and without having integrated back along the systems characteristic age τ_c. The right plot has values after backwards integration.

6.6 Simulating other sample progenitors

Having described the procedure for an example binary, we now proceed by merely stating the results of the entire binary run. Similar analysis was done for other systems, in particular the mentioned ones $J1811$, $J1756$, $B1534$ and the "Hulse-Taylor"-pulsar (it would not add much to the understanding by e.g. simulating both $B1913$ and $B2127$ as these have very similar eccentricity, orbital period and characteristic age). The results are stated below in terms of statistics.

Table 3: Statistics for the data obtained by simulating the progenitors. Note that the values for $\bar{\phi} = \pi$ and $\bar{\theta} = 0$ are just as would be expected, (that is antiparallel to v_1). The systems have not been integrated back in time. *Close* denotes as usual a limited deviation from the observed corresponding binary.

Designation	$\bar{v}_{kick}\ [km/s]$	$\sigma_{v_{kick}}\ [km/s]$	$\bar{\phi}\ [rad]$	$\sigma_{\phi}\ [rad]$	$\bar{\theta}\ [rad]$	$\sigma_{\theta}\ [rad]$
$J0737\ m_1 = 2.1\ M_{\odot},\ a = 1.18\ R_{\odot}$	276.26	252.16	3.14	1.48	0.00	0.67
$J0737_{close}\ m_1 = 2.1\ M_{\odot},\ a = 1.18\ R_{\odot}$	221.81	171.54	3.12	0.97	0.00	0.53
$J0737\ m_1 = 2.1\ M_{\odot},\ a = 1.40\ R_{\odot}$	257.04	232.39	3.13	1.47	0.00	0.67
$J0737_{close}\ m_1 = 2.1\ M_{\odot},\ a = 1.40\ R_{\odot}$	223.94	160.17	3.13	0.70	0.01	0.48
$J0737\ m_1 = 6.5\ M_{\odot},\ a = 1.40\ R_{\odot}$	702.24	283.31	3.14	0.45	0.00	0.42
$J0737_{close}\ m_1 = 6.5\ M_{\odot},\ a = 1.40\ R_{\odot}$	696.66	220.14	3.14	0.24	-0.02	0.42
$J0737\ m_1 = 4.5\ M_{\odot},\ a = 1.18\ R_{\odot}$	462.05	333.10	3.14	0.57	0.00	0.51
$J0737_{close}\ m_1 = 4.5\ M_{\odot},\ a = 1.18\ R_{\odot}$	577.81	275.67	3.17	0.39	-0.02	0.53
$B1913\ m_1 = 2.1\ M_{\odot},\ a = 1.07\ R_{\odot}$	293.60	266.67	3.14	1.54	0.00	0.67
$B1913_{close}\ m_1 = 2.1\ M_{\odot},\ a = 1.07\ R_{\odot}$	639.11	219.78	3.18	1.15	0.09	0.52
$B1913\ m_1 = 2.1\ M_{\odot},\ a = 4.66\ R_{\odot}$	164.76	112.82	3.14	1.40	0.00	0.69
$B1913_{close}\ m_1 = 2.1\ M_{\odot},\ a = 4.66\ R_{\odot}$	242.07	68.47	3.16	0.46	-0.04	0.26
$B1913\ m_1 = 3.7\ M_{\odot},\ a = 1.07\ R_{\odot}$	340.53	313.34	3.14	1.10	0.00	0.66
$B1913_{close}\ m_1 = 3.7\ M_{\odot},\ a = 1.07\ R_{\odot}$	710.90	214.43	3.34	0.96	0.14	0.42
$B1913\ m_1 = 6.5\ M_{\odot},\ a = 4.66\ R_{\odot}$	348.18	218.23	3.14	0.45	0.00	0.42
$B1913_{close}\ m_1 = 6.5\ M_{\odot},\ a = 4.66\ R_{\odot}$	519.67	107.51	3.25	0.23	0.00	0.19
$J1811\ m_1 = 2.1\ M_{\odot},\ a = 7.0\ R_{\odot}$	144.50	82.79	3.14	1.29	0.00	0.69
$J1811_{close}\ m_1 = 2.1\ M_{\odot},\ a = 7.0\ R_{\odot}$	241.07	78.15	3.34	1.29	0.07	0.37
$J1811\ m_1 = 2.1\ M_{\odot},\ a = 74.2\ R_{\odot}$	84.36	33.8	3.13	0.81	0.02	0.59
$J1811_{close}\ m_1 = 2.1\ M_{\odot},\ a = 74.2\ R_{\odot}$	75.01	13.80	3.16	0.23	0.02	0.19
$J1811\ m_1 = 6.5\ M_{\odot},\ a = 74.2\ R_{\odot}$	118.20	42.01	3.14	0.44	0.01	0.40
$J1811_{close}\ m_1 = 6.5\ M_{\odot},\ a = 74.2\ R_{\odot}$	125.72	15.21	3.12	0.15	0.01	0.12
$J1811\ m_1 = 6.5\ M_{\odot},\ a = 7.0\ R_{\odot}$	268.51	161.82	3.14	0.44	0.01	0.41
$J1811_{close}\ m_1 = 6.5\ M_{\odot},\ a = 7.0\ R_{\odot}$	311.66	72.27	3.10	0.83	0.15	0.30
$B1534\ m_1 = 2.1\ M_{\odot},\ a = 2.37\ R_{\odot}$	210.46	174.73	3.15	1.45	0.01	0.68
$B1534_{close}\ m_1 = 2.1\ M_{\odot},\ a = 2.37\ R_{\odot}$	288.8	169.5	3.06	1.17	-0.02	0.45
$B1534\ m_1 = 2.1\ M_{\odot},\ a = 4.17\ R_{\odot}$	167.43	117.74	3.15	1.36	-0.01	0.69
$B1534_{close}\ m_1 = 2.1\ M_{\odot},\ a = 4.17\ R_{\odot}$	197.65	86. 63	3.09	0.69	0.00	0.40
$B1534\ m_1 = 6.5\ M_{\odot},\ a = 4.17\ R_{\odot}$	382.03	225.89	3.14	0.42	0.00	0.40
$B1534_{close}\ m_1 = 6.5\ M_{\odot},\ a = 4.17\ R_{\odot}$	483.60	153.03	3.13	0.29	0.03	0.30
$B1534\ m_1 = 6.5\ M_{\odot},\ a = 2.37\ R_{\odot}$	542.31	275.73	3.13	0.43	0.00	0.40
$B1534_{close}\ m_1 = 6.5\ M_{\odot},\ a = 2.37\ R_{\odot}$	694.78	280.36	3.08	0.46	-0.03	0.40
$J1756\ m_1 = 2.1\ M_{\odot},\ a = 2.20\ R_{\odot}$	215.3	181.5	3.13	1.47	0.00	0.68
$J1756_{close}\ m_1 = 2.1\ M_{\odot},\ a = 2.20\ R_{\odot}$	242.7	154.7	3.20	1.15	0.00	0.49
$J1756\ m_1 = 2.1\ M_{\odot},\ a = 3.18\ R_{\odot}$	186.3	142.9	3.13	1.42	0.00	0.69
$J1756_{close}\ m_1 = 2.1\ M_{\odot},\ a = 3.18\ R_{\odot}$	210.7	122.1	3.11	0.75	0.00	0.45
$J1756\ m_1 = 6.5\ M_{\odot},\ a = 3.18\ R_{\odot}$	466.3	251.4	3.14	0.42	0.00	0.39
$J1756_{close}\ m_1 = 6.5\ M_{\odot},\ a = 3.18\ R_{\odot}$	582.0	188.0	3.14	0.27	0.00	0.38
$J1756\ m_1 = 6.5\ M_{\odot},\ a = 2.20\ R_{\odot}$	573.4	279.9	3.14	0.43	0.00	0.40
$J1756_{close}\ m_1 = 6.5\ M_{\odot},\ a = 2.20\ R_{\odot}$	639.6	236.0	3.12	0.40	0.00	0.45

From Table 3 above we can make a couple of observations. The mean deviations for the three kick parameters are invariably lower for the close systems. This is intuitively not surprising as the constraints impose a tighter range for the allowed kicks. We also comment that in all cases the close systems required an asymmetric (v_{kick} being non-zero) SN and that the angles ϕ and θ had to be within some range (they could not have been polar).

The difference of mean value for v_{kick} for the bound population compared to the close population can be both negative and positive. It seems that in the eccentric systems, that is $B1913$ and $J1811$, that the mean velocity is somewhat higher for the close systems. Furthermore, tighter systems have a higher $\bar{v}_{kick}$. This is of course not too surprising as a tighter binary would have a higher orbital velocity, thus requiring a higher kick magnitude to remain bound.

6.7 The role of the kick PDF

Having understood the above results with a given kick PDF, the we now vary the assumption of the kicks being distributed bimodally. Table 4 below gives the fractions of bound systems for the kick PDF presented by Hansen & Phinney (1997).

Table 4: Comparison of fraction of bound systems between the kick PDFs given by Arzoumanian et al. (2002) and Hansen & Phinney (1997).

Designation	Properties		$f_{bound}^{Hansen,Phinney}$	$f_{bound}^{Arzoumanian}$
$J0737$	$m_1 = 2.1\ M_\odot$,	$a = 1.17\ R_\odot$	65.2 %	53.1 %
	$m_1 = 2.1\ M_\odot$,	$a = 1.40\ R_\odot$	61.7 %	50.2 %
	$m_1 = 4.5\ M_\odot$,	$a = 1.17\ R_\odot$	30.7 %	23.4 %
	$m_1 = 6.5\ M_\odot$,	$a = 1.40\ R_\odot$	12.2 %	10.4 %
$B1534$	$m_1 = 2.1\ M_\odot$,	$a = 2.37\ R_\odot$	54.7 %	42. %
	$m_1 = 2.1\ M_\odot$,	$a = 4.17\ R_\odot$	43.6 %	34.2 %
	$m_1 = 6.5\ M_\odot$,	$a = 2.37\ R_\odot$	17.2 %	11.0 %
	$m_1 = 6.5\ M_\odot$,	$a = 4.17\ R_\odot$	18.8 %	9.9 %
$J1811$	$m_1 = 2.1\ M_\odot$,	$a = 6.97\ R_\odot$	33.7 %	29.0 %
	$m_1 = 2.1\ M_\odot$,	$a = 74.0\ R_\odot$	2.7 %	6.8 %
	$m_1 = 6.5\ M_\odot$,	$a = 6.97\ R_\odot$	21.5 %	14.5 %
	$m_1 = 6.5\ M_\odot$,	$a = 74.0\ R_\odot$	3.5 %	5.5 %
$B1913$	$m_1 = 2.1\ M_\odot$,	$a = 1.06\ R_\odot$	72.7 %	58.0 %
	$m_1 = 2.1\ M_\odot$,	$a = 4.48\ R_\odot$	42.5 %	34.5 %
	$m_1 = 3.8\ M_\odot$,	$a = 1.06\ R_\odot$	48.6 %	42.1 %
	$m_1 = 6.5\ M_\odot$,	$a = 4.48\ R_\odot$	20.5 %	11.2 %
$J1756$	$m_1 = 2.1\ M_\odot$,	$a = 2.20\ R_\odot$	56.5 %	44.6 %
	$m_1 = 2.1\ M_\odot$,	$a = 3.17\ R_\odot$	49.4 %	38.3 %
	$m_1 = 6.5\ M_\odot$,	$a = 2.20\ R_\odot$	15.8 %	10.5 %
	$m_1 = 6.5\ M_\odot$,	$a = 3.17\ R_\odot$	17.4 %	9.9 %

Also here the result is rather straight forward; in most cases the fraction of bound systems is somewhat higher for the unimodal PDF. This is not too surprising as the main range for the systems to remain bound are at lower kick velocities, which in the unimodal PDF have a higher probability density. Conversely, if one inspects the large separation of $J1811$ the result is the reverse. This is also explicable in terms of different probability densities, as the bimodal PDF has somewhat a higher density distribution at very low kicks.

We observe that in general the difference of bound systems are around 10 %, which gives us an estimate of the uncertainties caused by the kick PDFs. Furthermore they give implications for the Short gamma ray bursts. Depending on the kick PDF one would from population synthesis obtain a difference in merger rates, although the order of magnitude would probably not change.

7 Population synthesis

With the results in the above section we understand which progenitors produce the binaries that are actually observed. In this section we present results trying to compare the above results with some actual physics. We aim at comparing that which is expected from the known physics to what is actually observed. Using population synthesis, we derive the statistics of what the known physics imply. With this we then proceed by comparing this to the observed statistics of the current DNS population.

The first subsections concern discussion and description about the methodology, whereas the following sections present the results and then compare with above results.

7.1 Population synthesis

In order to do population synthesis, one must obviously start at a certain point in the formation channel. As the point is to obtain statistics in the post-SN[1] variables and the intermediate stage is assumed to circularize the system, the first SN-event will not play importance. Thus, the population synthesis can start with having the system consist of an already formed NS and an MS star. This limits to an incomplete population synthesis, with the main reason being that by starting at this point we have neglected all the previous interaction, such as the MS-MS interaction through e.g. Roche-lobe overflow. As mentioned we however are only interested in the statistics for DNS binaries, which is essentially only determined by the intermediate stage separation and He-core mass.

Assuming this is the starting point, there are a couple of parameters that need to be assigned probability functions. At first there is the pre-SN separation a, which is a non-trivial matter. Most sources in the literature use a distribution constant in $\log(a)$, (that is $P(a) \propto \frac{1}{a}$), to simulate the *zams* separation. We use separations between $(100 - 1000)\, R_\odot$, where it is argued that the below the lower limit the stars will merge during the CE phase, whereas the upper limit ensures interaction between the RG envelope and the companion star. To coarse approximation, this distribution can be extended to the intermediate stage separation as well. As the NS mass can well be constantly given its "canonical" value of $1.4\, M_\odot$, the MS star is somewhat more non-trivial. One can assume that the MS mass distribution at the pre-SN event is proportional to the Kroupa (2002) distribution, although this is rather simplistic; as the *zams* mass follows this distribution, the amount of mass lost through stellar wind[2], which depends on mass and metallicity among other things, the subsequent mass distribution a somewhat different form. Furthermore there is also the binary interaction before the first supernova, involving Roche-lobe overflow and *Bondi-Hoyle* accretion.

Furthermore one must take into account the CE phase. There are mainly two issues here; first the amount of lost mass due to envelope expulsion, and secondly the inspiral. The second issue can be done by following the above mentioned *Webbink formalism* with suitable values for λ and η_{eff}. The first issue however, is somewhat less trivial. To understand the He-core mass as a function of zams mass is difficult, given the binary interaction, stellar wind mass expulsion and later hydrogen fraction.

Finally the kick-distribution can be simulated using either of the above mentioned distributions.

7.2 Description of methodology for population synthesis

The population synthesis simulations are somewhat more straight-forward. Assuming a circularized system with an NS of $m_{NS} = 1.4\, M_\odot$ and a MS star, the separation is taken from the above mentioned distribution, the mass is taken from the ordinary IMF-distribution.

The common envelope is simulated using the *Webbink formalism* following the formulas in Section 2, with values for λ and η_{eff} being 0.5 and 1.0 respectively. The He-core mass as function of the zams mass is crudely taken to be a linear function from the mass range $(12 - 25)\, M_\odot$, which is the presumed mass range for binaries to give rise to NS, to the He-core mass range $(2.1 - 8)\, M_\odot$. The system has must

[1] In this context, the SN denotes the second supernova event.

[2] Massive NS progenitors, that is O- and B-type stars, lose mass in the order of $\dot{M}_* \sim 10^{-5}\, M_\odot/yr$, which is considerably more than e.g. that of the sun, which has a yearly mass loss of $\dot{M}_* \sim 10^{-14}\, M_\odot/yr$. Thus, when the older companion has passed through its MS-phase the mass lost through stellar wind will be considerable.

not suffer inspiral-merging, and thus a system is discarded if it fills its Roche-lobe after inspiral. This is done by using the He-core radial function of mass given by Tauris & van den Heuvel (2003), which considering that this formula is a *zero age He-core* radial formula should be a very good fit. The system is also discarded if the He-core has a mass superceding $6.5\,M_{\odot}$ as this is thought to lead to unstable mass transfer and merging in the intermediate stage.

From here the systems are kicked, with the same technique used for the progenitors. The program *PopSynth.java* keeps the bound systems and thus produces a population of DNS binaries.

7.3 The obtained statistics

With the above code the below results were obtained. The fraction of systems yielding a DNS binary were $\approx 28.7\,\%$.

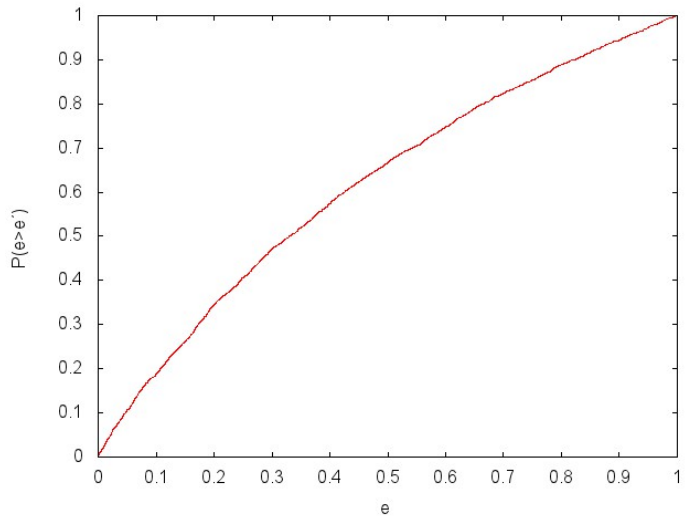

Figure 18: Cumulative plot of post-SN eccentricity.

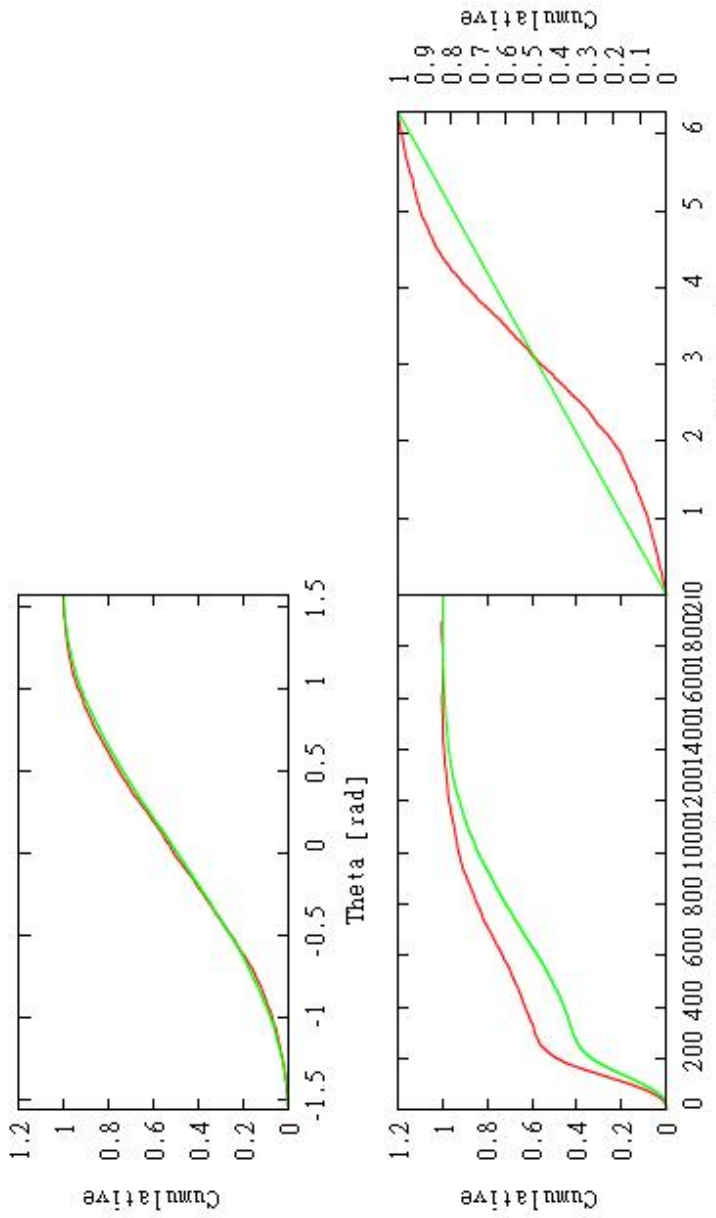

Figure 19: Comparisons of cumulative plots for the kick parameters. The v_{kick} PDF is given by Arzoumanian et al. (2002). The red line denotes the cumulative distribution of the synthesized bound systems. The green line gives the corresponding kick PDF or in the case of the angles, the isotropic distribution.

Figure 20: Statistical relations between various parameters for the conducted population synthesis. $a\prime$ denotes the binary separation after the second SN kick and a the separation after the common envelope.

The above results show interesting morphology; in the case of the cumulative plots, presented in Figure 19 we observe that the difference in v_{kick} is that the population synthesized bound systems show a preference towards lower kick-velocities. One would not be surprised over such a result; any kick PDF would be "distorted" in this way since there will always be a preference towards lower kick-velocities due to the lower kicks having higher probability of not disrupting the system.

Perhaps the nontrivial observation concerns that of the angles. We observe that in ϕ there is a non-isotropic preference towards the kicks being anti-parallel. The reason is trivially that for the anti-parallel case a higher fraction of the systems remain bound. As one would expect, the ϕ plot shows of a more concentrated distribution around $\phi = \pi$. The θ distribution show effectively no deviation from the isotropy.

The most important observation however, is that the plots show that indeed, although the cumulative plots show a higher concentration around the backwards direction, there are still systems being bound with $\phi = 0$ or polarly inclined kicks.

7.3.1 The role of the kick PDF

Having the above results for the Arzoumanian et al. (2002) kick PDF we now investigate whether the role of the kick PDF is of importance in the population synthesis. Using the same methodology as above, except with the kick PDF presented by Hansen & Phinney (1997), the results presented in Figure 21 were obtained. The fraction of systems becoming DNS binaries were $\approx 34.2\,\%$.

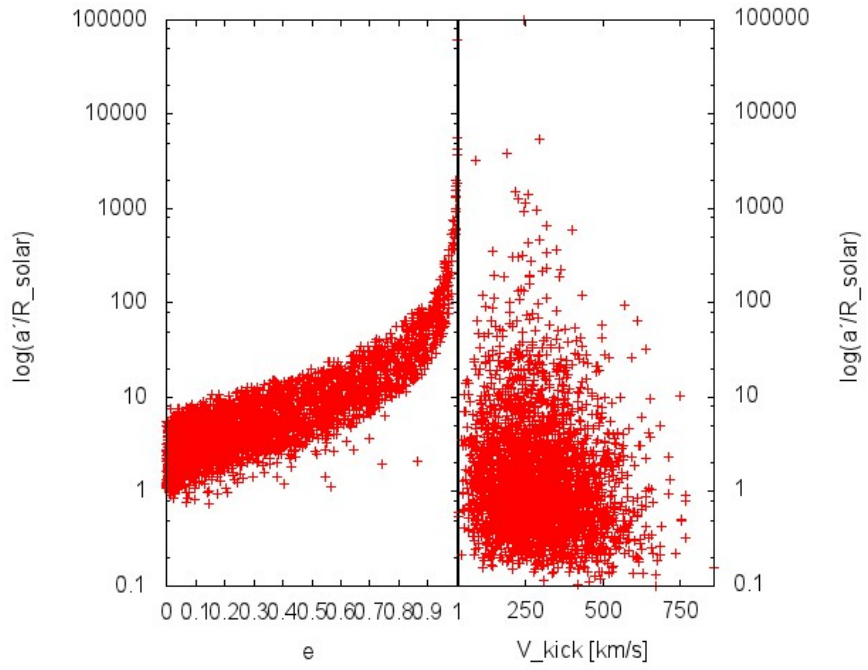

Figure 21: Population synthesis plot comparing $a\prime$, the post-SN separation, to the post-SN eccentricity, but now with the kick PDF given by Hansen & Phinney (1997).

The difference is perhaps trivial in the $a\prime$-v_{kick} diagram; the distribution of v_{kick} resembles the density profile of the kick PDF by Hansen & Phinney (1997) as one would expect. The second diagram however yields a slight hint; compared to the same plot, but with the bimodal distribution the case seems to be that the "underside" of the shape is missing. As the main difference between the unimodal PDF and the bimodal PDF is the higher probability density for higher kicks in the bimodal one, the difference must correspond to lack of high velocities. See Figure 22 for a comparison of PDFs.

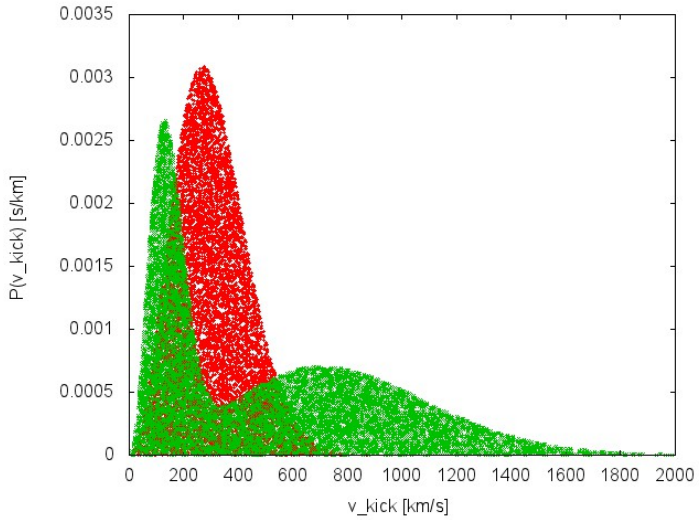

Figure 22: Plot of both the PDF given in Arzoumanian et al. (2002) and Hansen & Phinney (1997). Note the relatively high probability density of the bimodal distribution at high velocities.

7.4 Comparison to observation

We now proceed by comparing the the expected statistics from the population synthesis with the observed physics. The comparison is made as follows. Consider two systems with merger time ratio of 10. Then one would expect there to be ten more of the systems with the shorter merger time to have been around. Thus, to conduct the comparison we take the "close" systems of each progenitor and do weighted plots with these in cumulative diagrams. The weights are a product of two under-weights. First for each observed binary we weight with $1/\tau_{merger}$ so as to correspond to the statistics one would expect from the observed DNS population. Furthermore we weight with $1/N_i$ where N_i are all the "close" systems for some observed binary i (needless to say we also normalize the weight). The latter weight makes sure the statistics are unaffected by the number of "close" systems obtained for one binary. Thus the weight, given an observed binary, will be

$$\Delta P_j^i = \frac{(1/\tau_{merger})(1/N_i)}{\sum_k (1/\tau_{merger_k})}$$

where i is an observed binary, j is a "close" system and k runs over all the observed binaries. Note that the weight is equal for all "close" systems.

Below are presented the results.

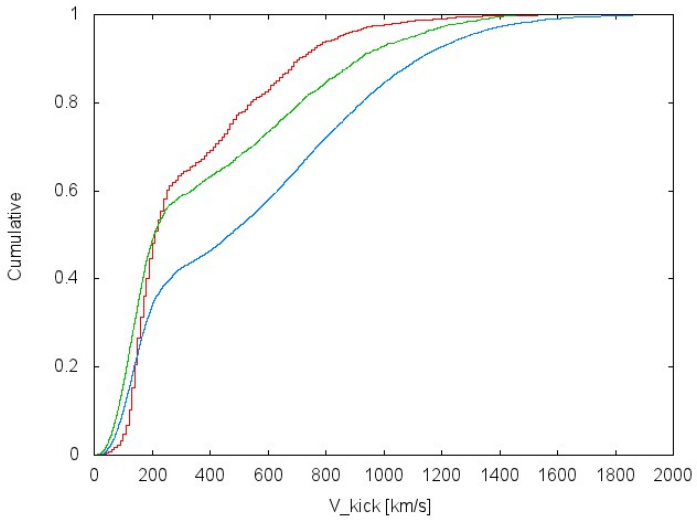

Figure 23: Comparison of cumulative distributions for the PDF given by Arzoumanian et al. (2002), the population synthesis conducted and the weighted progenitor systems becoming close to the observed current DNS systems. The first is depicted in blue, the second in green and the latter in red.

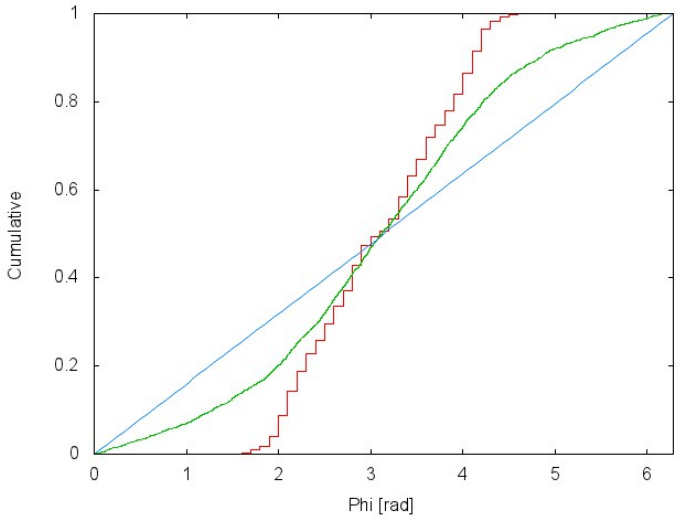

Figure 24: Comparison between the isotropic distribution of ϕ, the cumulative plots of ϕ for the synthesis and that of the close populations. The first is depicted in blue, the second in green and the latter in red.

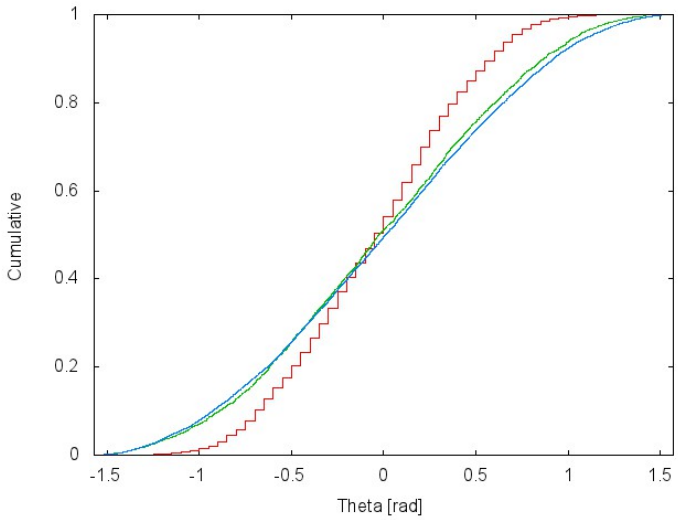

Figure 25: Comparison between the isotropic θ distribution, the cumulative plots of θ for the population synthesis and that of the close populations. The first is depicted in blue, the second in green and the latter in red.

The plots show interesting deviations from the population synthesis. The angular cumulative plots show in the case of ϕ a strong preference towards $\phi = \pi$, whereas that of θ shows a less strong planar preference. If one inspects the ϕ plot, one sees that the back-wards direction $\phi = \pi$ is very unlikely. This is in agreement with the observed morphology in the $\phi - v_{kicks}$-diagrams showing preference for close systems to be dense somewhat "outside" of $\phi = \pi$.

Some of these results are not suprising with the plots presented in previous sections in mind. The presented plots for $J0737$ give a clear maximum deviation from $\phi = \pi$ and $\theta = 0$ for the system to remain close, which explains why there are absolutely no systems outside of a given angular interval.

The v_{kick} cumulative diagram is also interesting. As mentioned, the PDF given by Arzoumanian et al. (2002), the v_{kick} of the population synthesis as well as the $1/\tau_{merger}$ weighted systems are plotted. The difference between the population synthesized distribution and that of Arzoumanian et al. (2002) is not too great; obviously the former shows preference to low kicks, which is not surprising and would have been the result of any kick PDF. This difference is rather a consequence of the rather obvious bimodal formation channel for the singleton NS used as sample by Arzoumanian et al. (2002). The difference between these two and that of the weighted progenitors close to the observed systems are, however, the less trivial observation. An inspection immediately yields the conclusion that essentially half of the systems have kicks ranging between $(100 - 200)\ km/s$, with the above velocities not diverging too much from the bimodal PDF. We interpret this as an indication that the currently available PDFs are too biased towards higher kick velocities.

Although our performed population synthesis gives that we should observe systems with very high polar kicks and parallel kicks we do not observe these in Nature. The plots hint that the angular PDF may not be isotropic, at least not from the observed sample. It should be noticed however, that the currently known DNS binary sample is rather scarce and a better analysis could be obtained if one had better knowledge of the unusual systems.

Furthermore, the results seem not to comply with the Dewi et al. (2005) spin-period eccentricity relation, as the major contribution of kicks comes from higher kick velocities. Furthermore the currently observed systems have, besides the three highly eccentric systems $J1811$, $B1913$ and $B2127$ in general a low eccentricity, which is hinting of a lower kick ($< 100\ km/s$), which also seems not to be in agreement with the above result. It should me emphasized also here, that this result is likely due to the scarce nature of the observed DNS binaries.

8 Summary and Conclusions

With the results in the above two sections we are now ready to draw our conclusions and summarize what we have done. We begin with the results regarding the progenitor analysis and continue concluding the population synthesis.

8.1 Kick constraints

We have constrained the kicks by first contraining the allowed progenitor phase space. This was done by constraining the phase space by mass and separation. We investigated our plotted results and found that the systems that had post-SN parameters sufficiently close to the corresponding system in all cases must have had a roughly anti-parallel kick, with the difference being comparatively small.

From here we proceeded by considering various effects by varying our assumptions. We first investigated the role of the systems age; that is to say we integrated the systems backwards in time, following the Peters (1964) differential equations for loss of separation and eccentricity through emission of GW. The results showed very little difference. We concluded that our analysis was on the whole affected very little by correcting for inspiral time.

8.2 Population synthesis

Furthermore, we have conducted population synthesis. Having understood the progenitor phase space and seen what they imply for the kicks, we proceeded by trying and reproduce certain relations throught the already known physics. We took as "starting point" in the binary evolution the circularized NS plus He-core situation were we simulated the separation and M_{MS} by the commonly used PDFs. The CE phase was simulated following the Webbink formalism, with typical values for λ and η_{eff}. We coarsely approximated the mass loss from zams star to He-core by a linear mass loss fit and kicked the systems using the bimodal PDF given by Arzoumanian et al. (2002). The results showed, when comparing the cumulative distribution of v_{kick} a preference towards lower kicks. We concluded that this was as would be expected as the population synthesis would, for any PDF, reduce the probability density of the higher kicks as these would have a lower probability of being bound. Furthermore there was distortion in the cumulative frequency of the angles, that is the angular distributions did not remain isotropic through the population synthesis. We varied the kick PDF and found that there was a little difference in the fraction of bound systems, agreeing with what we did in section 6.7. We conclude that this does not alter the results of the population synthesis much.

We compared our population synthesis with weighted simulated systems. This was done by taking the "close" systems of each simulation and weighting these with $1/\tau_{merger}$ so as to give a more realistic population. We found a rather interesting distinction between the population synthesis and the weighted close observed population. The angles showed a preference towards the anti-parallel direction, with no specimen outside some fixed range around $\phi = \pi$ and $\theta = 0$. We concluded that this was not in disagreement with the expectations, but also argued that since our population synthesis implied that there should exist binaries with very polarly or parallel kicks, the fact that we have yet to observe this implies that the current DNS population points towards a non-isotropic distribution.

We argued further that these results have interesting implications for the spin period - eccentricity relation found by Dewi et al. (2005). We saw that the main population from the weighted observed close systems are within $(100 - 200)\ km/s$, which is in direct disagreement with their initial assumption of very low magnitude second SN kicks. We mentioned that this may be due to the fact that the observed DNS population may be completely coincidental, as argued in the mentioned paper. Furthermore we mentioned that this is probably due to a bias towards high kick velocities in the current kick PDFs.

8.3 On the question set out to be answered

We recall now the question set out to be answered in the introductory section about what we can learn about the kicks from the observed DNS binary sample and in particular the angular distribution. We conclude that we have learned a lot, and in particular that the kick-distribution seems not to be isotropic.

9 Biases in assumptions and possible extensions

Having concluded our work, we now consider the validity of the assumptions used. We discuss certain simplifications and propose improvements and extensions.

9.1 Errors in data

As stated in Table 1, the various NS data have rather uncomfortably large error margins, in particular the companion masses of binaries $J1811-1736$ and $J1518-4904$, which are $1.06\,M_\odot$ and $1.05\,M_\odot$ respectively. These values are rather low for NSs and are with great certainty wrong. Following Kiziltan et al. (2010) the likely mass would be, with slight possible deviation, around $1.35\,M_\odot$. It is another matter however, whether these data would change the outcome of statistics. Comparing the $\tilde{m}$ for either $m_1\prime = 1.05\,M_\odot$ and $m_1\prime = 1.40\,M_\odot$ gives for e.g. $m_1 = 4.5\,M_\odot$ the approximate values 2.4 and 2.1 respectively. Inspecting the post-SN total energy equation from Section 5 it we draw the conclusion that it probably is of importance, but that our main conclusions remain the same.

Analogously the error margin in separation is negligible; as we saw when comparing the systems with and without time-integrated values the differences was very small and thus every conclusion remains unchanged.

9.2 The PDFs and isotropy

We varied our choice of kick PDF between that of Arzoumanian et al. (2002) and Hansen & Phinney (1997) and found in some cases considerable differences. It should be noted that the PDFs as given by the above authors do not really correspond to that of the kick velocity. The reasons are mainly two-fold; first any NS escaping the systems potential would lose some of its kinetic energy escaping the potential of the binary. Secondly, in the case of the bimodal distribution the bimodality is with all likelihood due to two different evolutionary scenarios. This would imply for our case that it might be better to choose one of the two distributions[1].

Furthermore we used an isotropic kick PDF and concluded that the angular distribution was not isotropic. This is of course a simplification. It is however not likely that the altering of the angular distribution would change the results much. Most systems in the observed population was probably produced by a planarly inclined kick and thus the number of "close" systems would only increase. The change would lead to the cumulative distribution given in Figure 19 being more concentrated around $\theta = 0$, which in turn would only strengthen our conclusion.

We propose as a next step to do an iteration process to find our own PDF for both the kicks and the angular distribution. The PDF iteration process should converge to a self-consistent solution; i.e. when conducting population synthesis with the PDFs the results should preserve the PDFs.

9.3 Spin alignment

Another thing to extend the analysis with is the spin alignment. As already discussed, the intermediate stage Roche lobe overflow tends to align the spin angular momentum vectors of the He-core and the NS to the orbital angular momentum plane. When the He-core undergoes SN its angular momentum will probably change (as it did in $J0737$). The older NS will however not change its angular momentum. This can be used to constrain the θ angle in the second SN kick. That is, if the angle between the post-SN orbital angular momentum and the older pulsar spin is known, one could use the older SN spin angular momentum angle as the indicator of how the pre-SN plane was configured, and thus measure the difference between the pre- and post-SN orbital angular momentum. Whence this relation is obtained, one could just include this into the code we used in the above simulations, thus constraining the kick further. The problematics here is that the angle ν is not known for all systems.

[1] Recall that the Arzoumanian et al. (2002) distribution is a linear combination of two Maxwellian distributions.

9.4 Weighted phase space simulation

In the above simulations the progenitors were taken from the "corners" of the given phase space. There are essentially two things wrong with this. First, the corners were equally weighted, which is an over-simplification, and secondly a better approach should be to simulate over the entire phase space and not only the corners. The natural extension to the latter one would be to randomize pairs of m_1 and a. For each such pair one would then construct the system, as done for each of the four cases individually in the above used code, and then run many kicks.

The issue would be sharpened even more if one could weight the systems. The higher mass would, of course, be less probable according to the Kroupa (2002) IMF distribution and the same goes for the separation. The weighting procedure would be somewhat non-trivial, but since the procedure would only concern relative probability one could do the weights as follows. Construct the phase space into a discrete space, that is m_1 and a on a lattice. Denote the weight of the lowest separation and lowest mass point w_0. The problem now is how to construct the weights for the other points on the lattice relative to w_0. For each of the phase space points $(m_\star, a_\star)$ one can choose the square $K_\star$ with the phase space point at its center. Given probability functions $P_m(m)$ and $P_a(a)$, for the mass and separation respectively, one could consequently integrate these over the square. Do this for the square around w_0 and the arbitrary one and divide, such that

$$\frac{w_\star}{w_0} = \frac{\int\int_{K_\star} P_a P_m \, dm \, da}{\int\int_{K_0} P_a P_m \, dm \, da}$$

If the probability functions for a and m_1 are independent of each others variables, the double integral will simply the products of the integrals.

From here and on the methodology would be simple: For the lowest corner in the lattice, simulate N binary systems as above, where N is chosen large enough so as to get good statistics. Proceed by for each other phase space pair on the lattice, simulate $\frac{w_\star}{w_0}N$ number of systems.

The probability functions could coarsely be taken to be the *IMF* for the mass and the inverse function for a. Knowing the envelope mass loss as a function of zams mass, one could then relate the probability of a He-mass directly to the IMF. Furthermore, the same arguments could be applied to a. Using the Webbink formalism one could find the final separation as a function of the zams mass (knowing the subsequent loss of hydrogen) and thus relate the inverse PDF for separation to the He-core NS system separation PDF.

With these simulations, one would have better understanding of the mass and separation dependence, but the main consequence would be the comparison to the population synthesis.

9.5 Intermediate stage binary interaction

With the understanding that the intermediate stage binary interaction is of importance, we now propose how one could do this. The intermediate stage (IS) interaction has been modeled by various authors, in particular by Dewi & Pols (2003). In their paper they describe, for various masses and separations, the subsequent evolutionary scenario. They present results in tables, with each entry giving the contact time, and the transferred mass. With the above recommended lattice approach, this would work very nicely as one could approximate for each phase space point the nearest corresponding table entry. They give the value of $\dot{M}_{He,max}$ for each case, and also the interaction time. The effect on the system of mass transfer can be described by the change of angular momentum. The effect of non-conservative mass loss of one of the components in a circularized system can be described by taking the logarithmic derivative. From section 5 there follows that the orbital angular momentum is

$$L_{orb} = v_{orb}(a_1 + a_2)\frac{m_1 m_2}{m_1 + m_2} = \frac{m_1 m_2}{m_1 + m_2}\sqrt{G(m_1 + m_2)/a^3}a^2$$

Denote the orbital angular momentum by $L_{orb} = J$. The logarithmic derivative gives

$$\frac{\dot{a}}{a} = 2\frac{\dot{J}}{J} - 2\frac{\dot{m}_1}{m_1} - 2\frac{\dot{m}_2}{m_2} + \frac{\dot{m}_1 + \dot{m}_2}{m_1 + m_2}$$

Moreover, $\dot{J}$ have contributions from gravitational waves emission of angular momentum, and the non-conservative mass loss. That is[1] $\dot{J} = \dot{J}_{massloss} + \dot{J}_{GW}$. It is reasonable to assume that $\dot{J}_{GW} << \dot{J}_{massloss}$ in the Roche-lobe overflow case. Following the arguments given in Tauris & van den Heuvel (2003) the latter term can be approximated with

$$\frac{\dot{J}_{massloss}}{J} = \frac{\alpha + \beta q^2 + \delta\gamma(1+q)^2}{1+q}\frac{\dot{m}_2}{m_2}$$

where α, β, γ and δ are constants in the paper and q the usual mass ratio. Assuming that the orbit remains circular the change in angular momentum can be used to model the effect of the IS Roche-lobe overflow.

This would increase the accuracy of the population synthesis and it is possible that the statistics would be somewhat altered; as the IS interaction give rise to non-conservative mass-transfer the allowed final mass range for the He-core will change somewhat.

9.6 Improving on the Webbink formalism

In the above simulations we used, without exception, the values $\eta_{eff} = 1.0$ and $\lambda = 0.5$. Though most sources in the literature use these values, they are somewhat of an oversimplification; there are different values for these parameters depending on the situation. This would be e.g. the metallicity of the stars, or the stage of which the star is in when interacting with the NS. An improvement could be to split up the different areas of the phase space and for each argue where what the proper parameters are. Although more accurate, it is doubtful whether this would to greater extent alter the conclusions.

[1] There are other interactions too; the mentioned paper gives that there is also effect due to magnetic braking and exchange due to one star expanding. We don't mention these here as they have been completely neglected throughout the work and furthermore they can also be neglected in this context as the GW-effect can.

A Derivation of inspiral-time formula from General Relativity

It can be shown from General Relativity, as done by Peters (1964), that the decrease of the semi-major axis a by emission of gravitational waves in a compact binary satisfies the following relation

$$\frac{da}{dt} = -\frac{64G^3 m_1 m_2 (m_1 + m_2)}{5a^3 c^5} \frac{(1 + e^2 \frac{73}{24} + e^4 \frac{37}{96})}{(1 - e^2)^{\frac{7}{2}}}$$

For the circular case, that is $e = 0$, this equation can be integrated analytically to give the inspiral time. The above differential equation for circular orbits reduces to

$$\frac{da}{dt} = -\frac{64G^3 m_1 m_2 (m_1 + m_2)}{5a^3 c^5} \Leftrightarrow a^3 \frac{da}{dt} = -\frac{64G^3 m_1 m_2 (m_1 + m_2)}{5c^5}$$

which can easily be integrated as follows:

$$\int_{t=0}^{t=\tau_{inspiral}} a^3 \frac{da}{dt} dt = \frac{1}{4}(a(\tau_{inspiral})^4 - a_0^4) = -\frac{1}{4} a_0^4$$

as $a(\tau_{inspiral}) = 0$ per definition. But there is also

$$\int_{t=0}^{t=\tau_{inspiral}} a^3 \frac{da}{dt} dt = \int_{t=0}^{t=\tau_{inspiral}} -\frac{64G^3 m_1 m_2 (m_1 + m_2)}{5c^5} dt =$$

$$= -\tau_{inspiral} \frac{64G^3 m_1 m_2 (m_1 + m_2)}{5c^5}$$

This manipulated gives

$$\tau_{inspiral} = a_0^4 \frac{5}{256} \frac{c^5}{G^3} \frac{1}{m_1 m_2} \frac{1}{m_1 + m_2}$$

B Lagrangian mechanics of a two-body system

Consider a two-body system with two masses m_1 and m_2 in a Newtonian potential with $U \propto r^{-1}$. As is well known within Classical Mechanics, this potential leads to elliptic orbits. In order to derive the eccentricity as a function of the variables one could consider the Lagrangian, which is in the natural terms

$$\mathcal{L} = E_k - E_p = \frac{1}{2}m_1\dot{r}_1 + \frac{1}{2}m_2\dot{r}_2 - G\frac{m_1 m_2}{|r_1 - r_2|}$$

The calculations will become simpler after a transformation to the CM frame, in which the Lagrangian has the following appearence:

$$\mathcal{L}_{CM} = \frac{1}{2}\frac{m_1 m_2}{m_1 + m_2}\dot{r}^2 + G\frac{m_1 m_2}{|r|} = \frac{1}{2}\mu\dot{r}^2 + G\frac{m_1 m_2}{|r|}$$

with the definitions $r \equiv r_1 - r_2$ and $\frac{m_1 m_2}{m_1+m_2} = \mu$ as usual being the reduced mass. The interpretation of the above Lagrangian is that of a particle with mass μ moving around a body at rest with mass $(m_1 + m_2)$. Since the Lagrangian contains only radial terms, it carries $SO(3)$-symmetry and Noethers theorem thus guaranties a conserved current. In this case it is the angular momentum. Thus one can choose to represent the system in a plane and in particular the masses by planar-polar coordinates. Therefore, put $r = (x, y) = (r\cos\phi, r\sin\phi)$ where it follows that

$$\dot{r} = (\dot{x}, \dot{y}) = \dot{r}(\cos\phi, \sin\phi) + r(-\sin\phi\dot{\phi}, \cos\phi\dot{\phi})$$

As the two vectors in $\dot{r}$ are orthonormal, the absolute value is simply the sum of the squares of the individual linear coefficients: $|\dot{r}|^2 = \dot{r}^2 + r^2\dot{\phi}^2$. The Lagrangian then becomes

$$\mathcal{L} = \frac{1}{2}\mu(\dot{r}^2 + r^2\dot{\phi}^2) + G\frac{\mu(m_1 + m_2)}{r}$$

Since the system now has only two generalized coordinates in ϕ and r, the Lagrangian has to satisfy for both these variables, the generic Euler-Lagrange equation of motion;

$$\frac{\partial\mathcal{L}}{\partial p} - \frac{d}{dt}(\frac{\partial\mathcal{L}}{\partial\dot{p}}) = 0$$

where p is some generalized coordinate. For r, this becomes

$$0 = \frac{\partial\mathcal{L}}{\partial r} - \frac{d}{dt}(\frac{\partial\mathcal{L}}{\partial\dot{r}}) = \mu r\dot{\phi}^2 - G\frac{\mu(m_1 + m_2)}{r^2} - \frac{d}{dt}(\mu\dot{r}) = \mu r\dot{\phi}^2 - G\frac{\mu(m_1 + m_2)}{r^2} - \mu\ddot{r}$$

With the usual definition of angular momentum, $L = mrv = \mu r^2\dot{\phi}$, and the above interpretation of the Lagrangian, the above equation becomes

$$0 = \ddot{r} - \frac{L^2}{r^3\mu^2} + G\frac{m_1 + m_2}{r^2}$$

Now do the change of variables $u(\phi) \equiv \frac{1}{r(\phi)}$. It follows that

$$\dot{r} = -\frac{1}{u^2}\frac{du}{dt} = -\frac{1}{u^2}\frac{du}{d\phi}\frac{d\phi}{dt} = -\frac{L}{\mu}\frac{du}{d\phi}$$

where $\frac{d\phi}{dt} = \frac{L}{\mu r^2}$ was used. Moreover, there is

$$\ddot{r} = \frac{d}{dt}\dot{r} = \frac{d}{d\phi}(-L\frac{du}{d\phi})\frac{d\phi}{dt} = -\frac{u^2L^2}{\mu^2}\frac{d^2u}{d\phi^2}$$

These equations give, for the above equation of motion, that

$$0 = \frac{d^2u}{dt^2} + u - G\frac{(m_1 + m_2)\mu^2}{L^2}$$

This ODE has the solution

$$u = A\cos(\phi - \phi_0) + G\frac{(m_1+m_2)\mu^2}{L^2} \Rightarrow r = \frac{L^2}{G(m_1+m_2)\mu^2}\frac{1}{1+\frac{L^2 A}{G(m_1+m_2)\mu^2}\cos(\phi-\phi_0)}$$

The latter function can be expressed more neatly with the definitions $e = \frac{L^2 A}{G(m_1+m_2)\mu^2}$ and $r_{min} = \frac{L^2}{G(m_1+m_2)\mu^2(1+e)}$ so that

$$r = r_{min}\frac{1+e}{1+e\cos(\phi-\phi_0)}$$

Comparing with the hamiltonian $\mathcal{H}$ gives that the energy of the system is

$$E = \frac{1}{2}(\dot{r}^2 + r^2\dot{\phi}^2)\mu - G\frac{(m_1+m_2)\mu}{r} = \frac{1}{2}\frac{L^2}{\mu}(\frac{du}{d\phi})^2 + \frac{1}{2}u^2\frac{L^2}{\mu} - Gu(m_1+m_2)\mu$$

so that with the solution for r above the energy becomes

$$E = \frac{1}{2}\frac{L^2A^2}{\mu} - \frac{G^2(m_1+m_2)^2\mu^3}{2L^2} = \frac{1}{2}\frac{L^2A^2}{\mu} - \frac{G^2m_1^3m_2^3}{2L^2(m_1+m_2)}$$

so that solving for e gives

$$e^2 = 1 + \frac{2EL^2(m_1+m_2)}{G^2m_1^3m_2^3}$$

References

Abbott, B. P., Abbott, R., Acernese, F., et al. 2010, ApJ, 713, 671

Armitage, P. J. & Livio, M. 2000, ApJ, 532, 540

Arzoumanian, Z., Chernoff, D. F., & Cordes, J. M. 2002, ApJ, 568, 289

Belczynski, K., Kalogera, V., & Bulik, T. 2002, ApJ, 572, 407

Bhattacharya, D. & van den Heuvel, E. P. J. 1991, PhysRep, 203, 1

Brandt, N. & Podsiadlowski, P. 1995, MNRAS, 274, 461

Brown, G. E. 1995, ApJ, 440, 270

Chevalier, R. A. 1996, ApJ, 459, 322

Church, R. P., Levan, A. J., Davies, M. B., & Tanvir, N. 2011, MNRAS, 413, 2004

Dewi, J. D. M., Podsiadlowski, P., & Pols, O. R. 2005, MNRAS, 363, L71

Dewi, J. D. M., Podsiadlowski, P., & Sena, A. 2006, MNRAS, 368, 1742

Dewi, J. D. M. & Pols, O. R. 2003, MNRAS, 344, 629

Dewi, J. D. M. & Tauris, T. M. 2000, A&A, 360, 1043

Eggleton, P. P. 1983, ApJ, 268, 368

Farr, W. M., Kremer, K., Lyutikov, M., & Kalogera, V. 2011, ArXiv e-prints

Flannery, B. P. & van den Heuvel, E. P. J. 1975, A&A, 39, 61

Fryer, C. & Kalogera, V. 1997, ApJ, 489, 244

Fryer, C. L. & Kusenko, A. 2006, ApJS, 163, 335

Fryxell, B. A. & Arnett, W. D. 1981, ApJ, 243, 994

Hansen, B. M. S. & Phinney, E. S. 1997, MNRAS, 291, 569

Hobbs, G., Lorimer, D. R., Lyne, A. G., & Kramer, M. 2005, MNRAS, 360, 974

Hulse, R. A. & Taylor, J. H. 1975, ApJ, 195, L51

Johnston, S., Hobbs, G., Vigeland, S., et al. 2005, MNRAS, 364, 1397

Kalogera, V., Kim, C., Lorimer, D. R., et al. 2004, ApJ, 601, L179

Kiziltan, B., Kottas, A., & Thorsett, S. E. 2010, ArXiv e-prints

Kroupa, P. 2002, Science, 295, 82

Lattimer, J. M. & Prakash, M. 2010, ArXiv e-prints

Lorimer, D. R. 2008, Living Reviews in Relativity, 11, 8

O'Shaughnessy, R., Kim, C., Kalogera, V., & Belczynski, K. 2008, ApJ, 672, 479

Peters, P. C. 1964, Physical Review, 136, 1224

Sofue, Y., Honma, M., & Omodaka, T. 2009, PASJ, 61, 227

Tauris, T. M. & van den Heuvel, E. 2003, ArXiv Astrophysics e-prints

Waldman, S. J. 2011, ArXiv e-prints

Wang, C., Lai, D., & Han, J. L. 2006, ApJ, 639, 1007

Webbink, R. F. 1984, ApJ, 277, 355

Willems, B., Andrews, J., Kalogera, V., & Belczynski, K. 2008, in American Institute of Physics Conference Series, Vol. 983, 40 Years of Pulsars: Millisecond Pulsars, Magnetars and More, ed. C. Bassa, Z. Wang, A. Cumming, & V. M. Kaspi, 464–468

Wongwathanarat, A., Janka, H.-T., & Müller, E. 2010, ApJ, 725, L106

Zahn, J.-P. 1989, A&A, 220, 112

Zhang, C. M., Wang, J., Zhao, Y. H., et al. 2011, A&A, 527, A83+